CHEMISTRY OF MATERIALS

pubs.acs.org/cm

Perspective

Complex Dynamics in Argyrodite Solid-State Ion Conductors

Austin M. Shotwell, Shelby L. Galinat, and Annalise E. Maughan*

Cite This: *Chem. Mater.* 2026, 38, 3038−3058

Read Online

ACCESS | Metrics & More | Article Recommendations

ABSTRACT: Argyrodites are a compositionally diverse family of materials that exhibit remarkable ion transport properties. While the average crystal structures of argyrodites have been extensively studied, ion transport in these materials is governed by a confluence of dynamic processes spanning the cation, anion, and polyanionic sublattices. This Perspective synthesizes recent advances in understanding the role of dynamics in structural behavior and ion transport properties. We examine the compositional and structural motifs that govern order−disorder transitions within the argyrodite family and further explore how ion hopping is facilitated by lattice dynamics, from long-range phonons to local rotational dynamics of polyanionic species. Through the lens of dynamics spanning multiple time and length scales, we establish guiding principles that govern transport phenomena and highlight avenues of future study for the argyrodite family of ion conductors.

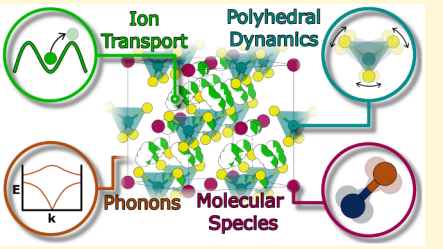

1. INTRODUCTION

The prototypical argyrodite, Ag_8GeS_6 (Figure 1), is a naturally occurring silver ore first identified by Albin Weisbach in 1885.[1]

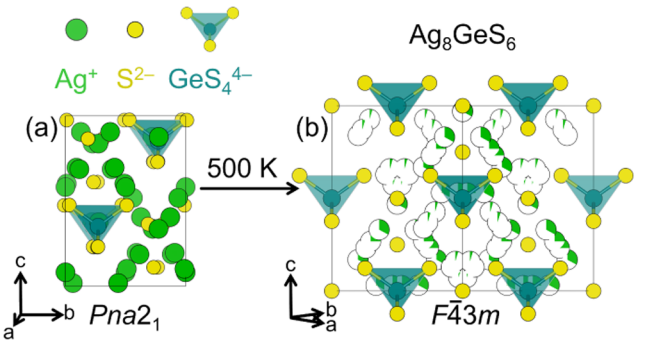

Figure 1. Low temperature (a) and high temperature (b) phases of Ag_8GeS_6. Below 500 K, Ag_8GeS_6 adopts a $Pna2_1$ structure with fully occupied Ag^+ sites. Above 500 K, Ag_8GeS_6 adopts the $F\bar{4}3m$ aristotypic argyrodite structure with highly mobile and delocalized Ag^+.

Ag_8GeS_6 served as a feedstock for the first successful isolation of elemental germanium by Clemens Winkler in 1886.[1] In recent decades, the argyrodite family has expanded to accommodate a wide range of chemistries, which have attracted attention for their optical properties,[2−9] thermoelectric behavior,[5,10−17] and their propensity for fast ion conduction.[18−32] Argyrodites are a compositionally diverse family of chalcogenides with the general form $A^{m+}_{(12-n-z)/m}M^{n+}Ch^{2-}_{6-z}X_z$ ($0 \le z \le 2$), where m and n are the charges of the A-cations (mono- or divalent) and M-cations (cations from groups 13−15 of the periodic table), respectively.[33] *Ch* is a chalcogenide, and X is a halide or pseudohalide.

Recent interest has been rekindled by Li_6PS_5X (X = Cl, Br, I) argyrodites and their high room-temperature ionic conductivities ($\sim 10^{-3}$ S cm^{-1}).[18,19] Through compositional tuning, these conductivities can be further enhanced into the $\sim 10^{-2}$ S cm^{-1} range, which is competitive with liquid electrolytes.[34−36] Ion transport properties of the argyrodites originate from a confluence of crystal structure, atomic disorder, and complex dynamics, including localized dynamics of polyanionic and molecular species as well as long-range vibrations in the form of phonons.

In this perspective, we integrate multiscale structural and dynamic insights to form a holistic understanding of the argyrodites as ion conductors. We first provide a structural overview of the argyrodite family, with particular emphasis on order−disorder phase transitions. We then discuss Arrhenius-type ion transport and review the prevailing structural picture of lithium-ion conduction in argyrodites. Building on this background, we analyze the influence of phonons on ion transport and highlight the critical role of the Arrhenius prefactor (σ_0) in ionic conductivity. Finally, we transition from collective, periodic dynamics to a local perspective, presenting rotationally active polyhedra and molecular species as key dynamic motifs that govern ion transport.

Received: October 31, 2025
Revised: March 10, 2026
Accepted: March 13, 2026
Published: March 27, 2026

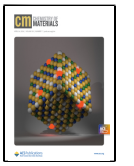

https://doi.org/10.1021/acs.chemmater.5c02939
Chem. Mater. 2026, 38, 3038−3058

2. THE ARGYRODITE STRUCTURE AND ITS DERIVATIVES

The uniting feature of the argyrodites is the adoption of a high temperature $F\bar{4}3m$ crystal structure with a disordered and highly mobile *A*-cation sublattice (Figure 1b).[33] Broadly, the $F\bar{4}3m$ argyrodite structure is composed of isolated MCh_4 tetrahedra separated by "free" Ch^{2-} and X^- (where compositionally appropriate). *A*-cations fill the interstices and commonly exhibit partial occupancies across multiple sites. The high temperature $F\bar{4}3m$ structure is considered an "aristotype" of the argyrodite family—a high-symmetry structure which represents the idealized version of lower-symmetry "hettotypes."[37] At low temperatures, various lower symmetry structures are observed (Figure 2a–c), depending on composition.[33,37] This hettotype-aristotype relationship is illustrated by comparison of the anion sublattices in three common low-temperature structures (Figure 2a–c) with that of the high temperature $F\bar{4}3m$ aristotype (Figure 2d). In all three hettotypes, the tetrahedral units exhibit slight orientational deviations from their positions in $F\bar{4}3m$, while the free chalcogenide sites show complementary modulations. The reduced mobility of cations in the low temperature hettotypes is reflected in localized cation arrangements (Figure 1a) and lower average symmetry.[33] Table 1 summarizes a selection of Ag^+, Cu^+, and Li^+ argyrodites, their room temperature structures, and their transition temperatures to the $F\bar{4}3m$ aristotype.

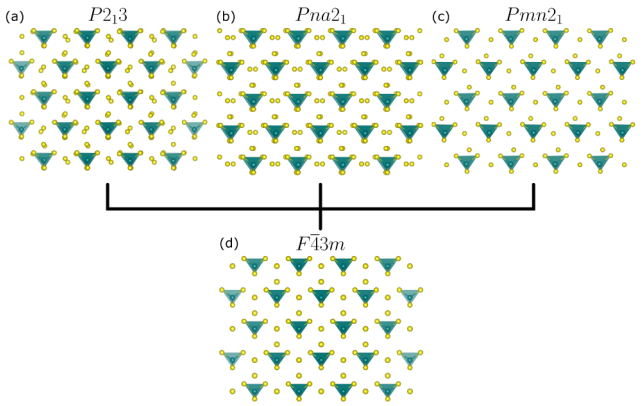

Figure 2. Anion sublattices of (a) $P2_13$ (Ag_7PS_6), (b) $Pna2_1$ (Ag_8GeS_6), (c) $Pmn2_1$ (Ag_8GeSe_6), and (d) $F\bar{4}3m$ (Li_6PS_5Br) argyrodites. Structures have been expanded and oriented to provide equivalent perspectives that emphasize the translational and rotational modulations that relate the hettotype lattices to the aristotype lattice. Cation sublattices have been omitted for clarity, but do differ between structures. In (d), the mixed S^{2-}/Br^- sites are colored uniformly yellow for ease of comparison to the hettotype structures.

The hettotype-aristotype relationship is best characterized as an order–disorder transition where translational dynamics of the cations and rotational dynamics of the MCh_4 units are activated. The high symmetry of the $F\bar{4}3m$ aristotype has long been attributed to dynamic averaging of the *A*-cation sublattice.[33] We hypothesize that this effect is also at play with the polyhedral anions. Our hypothesis is supported by recent local structure studies that demonstrate local symmetry breaking indicative of MCh_4 rotational dynamics or disorder in aristotypic Li^+ and Ag^+ argyrodites.[38−40] The same local-average structural deviations are not present in low-temperature hettotypes, indicating that disorder is activated upon transition to the aristotype.[39] Under this formulation, large librations of MCh_4 tetrahedra in the aristotype average to a coaligned and ordered motif (Figures 1b and 2d), while cation hopping is captured as partial occupancy over a wide range of sites (Figure 1b). Similar local-average structural deviations have been rationalized in β-Na_3PS_4 and $Na_{2.9}Sb_{0.9}W_{0.1}S_4$ as the effect of an order–disorder transition in which the cubic disordered phase dynamically samples various local tetragonal configurations, which average to long-range cubic symmetry.[41,42]

The local structure of Cu^+-argyrodites is still emerging. We are aware of one study in which temperature-dependent total scattering of Cu_7PSe_6 was collected on a laboratory diffractometer with limited resolution.[43] Notably, the pair distribution function (PDF) exhibited minimal change across the hettotype-aristotype phase transition. These changes were dominated by broadening of pair correlations that may be due to increased thermal displacement or activation of polyhedral dynamics.

The *A*-cation disorder associated with aristotypic argyrodites identified them as candidate ion conductors and prompted the search for variants that adopt the $F\bar{4}3m$ structure at room temperature.[33] Although introducing more polarizable chalcogenides often reduces the phase transition temperature (Table 1), such an approach does not reliably stabilize the aristotype at room temperature. In contrast, substitution of the chalcogenide with a halide (or pseudohalide) stabilizes the $F\bar{4}3m$ aristotype at room temperature across most compositions (Table 1).[33,44−46] Anion choice is strongly correlated with the amplitude of observed PS_4^{3-} rotational disorder in Li_6PS_5X ($X = Cl^-, Br^-, I^-$), which implies a link between MCh_4 disorder, anion identity, and phase behavior.[38] A similar effect is present in Na_3PO_4 and Na_3SbS_4 derivatives, where introduction of lower valence anions and the resulting cation vacancies stabilize high temperature phases characterized by local polyhedral orientational disorder.[41,42,47,48] The above observations suggest that weakening anion-anion interactions—through substitution of more polarizable chalcogenides or introducing monovalent halides—stabilizes the argyrodite aristotype by lowering the thermal energy required to activate dynamic disorder, which manifests in local-average structural disagreements.[38−40,49]

3. A BRIEF PRIMER ON SOLID-STATE ION TRANSPORT

In the crystalline solid state, ionic transport is commonly quantified by the Arrhenius framework, in which mobile ions hop between neighboring sites within the periodic structure along a minimum free energy pathway.[112−117] Between neighboring energetic minima, the ion must pass through an energetic saddle point corresponding to a geometric bottleneck between sites. This construction is rooted in absolute rate theory[118] and hopping conductivity is described by the Arrhenius relationship:

$$\sigma T = \sigma_0 \exp\left(-\frac{E_A}{k_B T}\right) \tag{1}$$

where σ is ionic conductivity, T is temperature, and k_B is the Boltzmann constant. The activation barrier (E_A) includes the enthalpy of migration (ΔH_m) and defect formation energy $\left(\frac{1}{2}\Delta H_f\right)$, while the Arrhenius prefactor (σ_0) represents temperature-independent contributions to ion transport:

$$\sigma_0 = \left(\frac{\gamma c \nu_0 Z^2 e^2 a_0^2}{k_B}\right) \exp\left(\frac{\Delta S_m}{k_B}\right) \tag{2}$$

https://doi.org/10.1021/acs.chemmater.5c02939
Chem. Mater. 2026, 38, 3038−3058

Table 1. Ag^+, Cu^+, and Li^+ Argyrodites with Their Room Temperature Space Groups and Hettotype-Aristotype Transition Temperatures[a]

Composition	Space Group at 298 K	$F\bar{4}3m$ Transition Temp (K)	Refs
		Ag^+	
Ag_9GaS_6	Body-centered orthorhombic	301−310	55−58
Ag_8GaS_5Cl	$F\bar{4}3m$	—	33
Ag_8GaS_5Br	$F\bar{4}3m$	—	33
Ag_8GaS_5I	$F\bar{4}3m$	—	33
Ag_9GaSe_6	$F\bar{4}3m$	281	59
Ag_8GaSe_5Br	$F\bar{4}3m$	—	33
Ag_8GaSe_5I	$F\bar{4}3m$	—	33
Ag_8SiS_6	$Pna2_1$	507	60, 61
Ag_7SiS_5Cl	$Pna2_1$	491	33
Ag_7SiS_5Br	$F\bar{4}3m$	—	33, 44
Ag_7SiS_5I	$F\bar{4}3m$	—	2, 33, 44, 62
Ag_8SiSe_6	$P2_13$[14] $Pmn2_1$[10,11]	370[14] 400[10,11]	10, 11, 14, 61
Ag_8SiTe_6	$F\bar{4}3m$	263	61, 63, 64
Ag_8GeS_6	$Pna2_1$	500	1, 61, 65, 66
Ag_7GeS_5Cl	$Pna2_1$	423	33
Ag_7GeS_5Br	$F\bar{4}3m$	—	33, 44
Ag_7GeS_5I	$F\bar{4}3m$	—	33, 44, 67
Ag_8GeSe_6	$Pmn2_1$	320−410[15] 321[61]	15, 61, 68
Ag_7GeSe_5Br	$F\bar{4}3m$	—	33
Ag_7GeSe_5I	$F\bar{4}3m$	—	31, 33, 69, 70
Ag_8GeTe_6	$F\bar{4}3m$	244	33, 61, 71
Ag_7GeTe_5I	$F\bar{4}3m$	—	33
Ag_8SnS_6	$Pna2_1$	460	72−74
Ag_7SnS_5Br	$F\bar{4}3m$	—	33, 44
Ag_7SnS_5I	$F\bar{4}3m$	—	33, 44
Ag_8SnSe_6	$Pmn2_1$	355	29, 68, 74
Ag_7SnSe_5I	$F\bar{4}3m$	—	33
Ag_7PS_6	$P2_13$	495,[33] 544[66]	3, 33, 66
Ag_6PS_5Cl	$F\bar{4}3m$	—	9
Ag_6PS_5Br	$F\bar{4}3m$	—	9, 33, 75
Ag_6PS_5I	$F\bar{4}3m$	—	75
Ag_7PSe_6	$P2_13$	453	76−78
Ag_6PSe_5Cl	$P2_13$	—	79
Ag_6PSe_5Br	$P2_13$	—	33, 79
Ag_6PSe_5I	$P2_13$	—	33, 79
Ag_7AsS_6	$P2_13$	523	33, 80, 81
Ag_6AsS_5I	$F\bar{4}3m$	—	33
Ag_7AsSe_6	$P2_13$	423	80
		Cu^+	
Cu_8SiS_6	$Pmn2_1$	336	17, 33, 60, 74, 82−85
Cu_7SiS_5I	$F\bar{4}3m$	—	33, 86
Cu_8SiSe_6	$Pmn2_1$	323−355	33, 74, 84, 85, 87
Cu_7SiSe_5I	$F\bar{4}3m$	—	33
Cu_8GeS_6	$Pmn2_1$	328−341	13, 33, 74, 88−90
Cu_7GeS_5I	$F\bar{4}3m$	—	7, 33, 86
Cu_8GeSe_6	$P6_3cm$	983	84, 89, 91
Cu_7GeSe_5I	$F\bar{4}3m$	—	7, 92
Cu_7PS_6	$P2_13$	510	12, 33, 93
Cu_6PS_5Cl	$F\bar{4}3m$	241	33, 45, 94, 95
Cu_6PS_5Br	$F\bar{4}3m$	268	33, 45, 94, 96
Cu_6PS_5I	$F\bar{4}3m$	268	45, 94, 96
Cu_7PSe_6	$P2_13$	320	33, 43, 97
Cu_6PSe_5Br	$F\bar{4}3m$	259	4, 16, 75
Cu_6PSe_5I	$F\bar{4}3m$	260−268	6, 16, 75
Cu_6AsS_5Br	$F\bar{4}3m$	—	5, 98
Cu_6AsS_5I	$F\bar{4}3m$	260−280	5, 8, 98
		Li^+	
Li_7GeS_5Br	$F\bar{4}3m$	—	99
Li_6PO_5Cl	$F\bar{4}3m$	—	100
Li_6PO_5Br	$F\bar{4}3m$	—	100
Li_7PS_6	$Pna2_1$	483	32, 46, 101, 102
Li_6PS_5Cl	$F\bar{4}3m$	—	18, 19, 32, 46, 103, 104
Li_6PS_5Br	$F\bar{4}3m$	—	18, 19, 32, 46, 103, 104
Li_6PS_5I	$F\bar{4}3m$	173	18, 19, 32, 46, 103, 104
$Li_6PS_5BH_4$	$F\bar{4}3m$	—	105, 106
Li_6PS_5CN	$F\bar{4}3m$	—	107, 108
Li_7PSe_6	$Pna2_1$	437	46, 101
Li_6PSe_5Cl	$F\bar{4}3m$	—	109
Li_6PSe_5Br	$F\bar{4}3m$	—	109
Li_6PSe_5I	$F\bar{4}3m$	—	110
Li_6AsS_5Br	$F\bar{4}3m$	—	46
Li_6AsS_5I	$F\bar{4}3m$	173	46
Li_6AsSe_5I	$F\bar{4}3m$	—	46
Li_6SbS_5I	$F\bar{4}3m$	—	34, 111

[a]Partial substitutions have been accomplished[20,25,34,50−54] but have been excluded for brevity.

σ_0 contains contributions from the dimensionality of ion conduction pathways (γ), number and charge of mobile carriers (c, Z), the elementary charge (e), the attempt frequency of ion hopping (ν_0), and the jump distance (a_0).[117,119,120] σ_0 is exponentially dependent upon entropy of migration (ΔS_m), which is determined (under the harmonic approximation) by the ratio of the vibrational partition functions associated with the mobile ion:[118]

$$\Delta S_m = k_B \ln\left(\frac{\prod_{j=1}^{N-1}\nu_j^0}{\prod_{j=1}^{N-1}\nu_j'}\right) \quad (3)$$

where the numerator is a product over $N-1$ normal modes of the system with the mobile ion in the equilibrium position and the denominator is a product over $N-1$ normal modes when the mobile ion is at the saddle point.[118]

The above relationships decompose temperature-dependent ionic conductivity into basic energetic terms, but imply discrete and entirely uncorrelated hopping processes. This framework does not necessarily hold for solid ion conductors in which ion motion is often highly correlated. This phenomenon is described by the Haven ratio, H_R:

$$H_R = \frac{D^*}{D_\sigma} \quad (4)$$

https://doi.org/10.1021/acs.chemmater.5c02939
Chem. Mater. 2026, 38, 3038−3058

where D^* is the tracer or self-diffusivity of a mobile ion and D_σ is the charge or conduction diffusivity calculated from ionic conductivity.[53,121−123] Self-diffusivity describes the ease with which a single mobile ion moves through the electrolyte, while the conduction diffusivity describes the macroscopic propensity for a material to move charge. In systems where the mobile species are either extremely dilute or completely noninteracting, $D^* = D_\sigma$ and $H_R = 1$.[121] $H_R < 1$ reflects positively correlated motion that enhances net charge transport, while $H_R > 1$ indicates negatively correlated or closed-loop motion that leads to low charge transport relative to self-diffusion.[122] Ceramic fast ion conductors often have H_R values of less than 1 and exhibit correlated motion that enhances charge transport.[53,121−123] While H_R indicates the presence of correlated motion, it provides minimal insight into the mechanistic character of correlation effects.[123] Li_6PS_5Cl is characterized by $H_R < 1$,[53,124] while a comparison of ionic conductivities estimated from nuclear magnetic resonance (NMR) spectroscopy and those determined via broadband impedance spectroscopy indicates that $H_R \approx 1$ in Li_6PS_5Br and $H_R \gg 1$ in Li_6PS_5I.[125]

Absolute rate theory assumes statistically independent hopping events, yet the deviation of the Haven ratio from unity may suggest that the Arrhenius framework is not suitable for describing correlated hopping events. In some systems, often "superionic" conductors, absolute rate theory breaks down and a "liquid-like" diffusive regime emerges.[126] The failure of absolute rate theory is indicated by a multiple orders of magnitude deviation of the rate prefactor obtained via NMR from the optical phonon frequencies of the crystal.[127,128] This behavior is not observed in the Li_6PS_5X (X = Cl^-, Br^-, I^-) argyrodites that are central to this work—ν_0 obtained from ^{7}Li NMR is within 1 order of magnitude of the Debye frequency ($\nu_D \simeq 10^{12}$ Hz), which provides an indicator of phonon frequency, for all three compositions.[18,49] In these systems, ion transport can be treated under absolute rate theory despite deviations of H_R from unity because diffusion proceeds via chain-like hopping rather than uncorrelated nearest-neighbor hops.[22,129] In anion-disordered phases (Section 4), long, open diffusion chains allow ΔH_f to be interpreted as the energy required to form Frenkel pairs separated by a chain length rather than adjacent defects.[129] In anion-ordered phases, closed diffusion chains within Li^+ cages (Section 4) produce high local mobility and low macroscopic conductivity, with Arrhenius behavior reflecting the rate-limiting transfer between cages.[22,125]

4. THE STRUCTURAL PICTURE OF ION TRANSPORT IN ARGYRODITES

Although this perspective primarily examines the dynamics of the argyrodites, it is important to first outline the structural basis of ion transport. Here we discuss how structure dictates ion transport in Li_6PS_5X (X = Cl^-, Br^-, I^-) and their derivatives. We focus our discussion on aristotypic Li^+-argyrodites due to the ubiquity of high-quality structural and electrochemical studies in these systems.[18−25,27,28,34,35,53,130] We highlight possible pathways for Li^+ hopping processes and establish the structure−property relationships that facilitate fast ion transport.

Fast ion conduction in argyrodites arises from formation of a percolating network of tetrahedral voids, commonly described by doublet, intracage, and intercage hops. The Li^+ sublattice consists of pseudo-octahedral cages centered at the 4*d* Wyckoff position (Figure 3a and b), whose vertices can host Li^+ and support rapid migration between clustered sites (doublet, Figure 3c).[21] While ion motion within cages is fast (≈10^9 s^{-1} at 329 K in Li_6PS_5I)[131] long-range transport is limited by intercage hops between neighboring cages. Understanding ion transport therefore requires resolving the possible physical pathways that collectively define these processes.

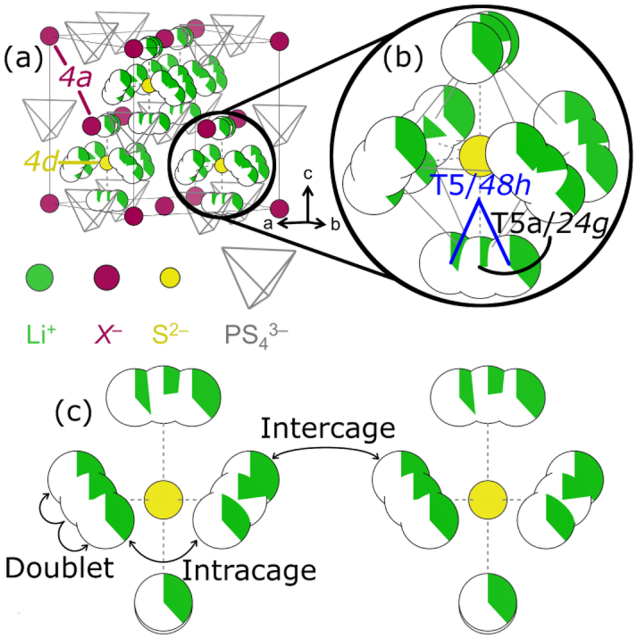

Figure 3. Illustration of (a) the structure of a Li_6PS_5X argyrodite exhibiting no S^{2-}/X^- antisite disorder. X^- occupies the 4*a* Wyckoff position on the faces and corners of the unit cell, while S^{2-} occupies the 4*d* positions on the interior of the unit cell. Li^+ is arranged in pseudo-octahedral cages on the 48*h* and 24*g* Wyckoff positions surrounding the 4*d* site (b). Cations can hop within and between cages (c). All three illustrated hop types are required for long-range ion transport.

Five tetrahedral sites (types 1−5) can accommodate Li^+ in argyrodites, with Li^+ most commonly observed on type 5 (T5, Figure 4a), type 2 (T2, Figure 4b), and type 4 (T4, Figure 4c) sites.[19,24,25,35,46,132] Significant Li^+ density is also found at the shared face of adjacent T5 sites (T5a), though it remains unclear whether this represents a true equilibrium site or time-averaged hopping between T5 positions.[19,132] T5 sites are coordinated by 4*a*, 4*d*, and two S^{2-} anions from distinct PS_4^{3-} units; T2 sites share a similar coordination but draw both S^{2-} from the same PS_4^{3-} unit, while T4 sites are coordinated by 4*a* and three S^{2-} from different PS_4^{3-} units. Minor occupation of T3 sites, which share faces only with T4, has been reported and may indicate a T4-T3-T4 pathway.[25,133] Within this framework, T5/T5a sites are treated as equilibrium positions, while T2 and T4 act as interstitial sites. Doublet hopping occurs directly between adjacent T5 sites, intracage hopping proceeds via T5-T2-T5, and intercage transport follows either T5-T2-T2-T5 (Figure 4d) or T5-T4-T5 (Figure 4e) pathways.[22]

Anion antisite disorder is a well-established materials design principle for high ionic conductivity in Li^+ argyrodites. Li_6PS_5I represents the anion-ordered case; I^- almost exclusively occupies the 4*a* Wyckoff position, while S^{2-} occupies the 4*d* Wyckoff position (Figure 3a), which has been attributed to the large ionic radius of I^-.[18] In contrast, Li_6PS_5Cl and Li_6PS_5Br exhibit S^{2-}/X^- antisite disorder— the 4*a* and 4*d* sites exhibit partial occupation of both S^{2-} and X^-.[18] The presence of anion site mixing in Li_6PS_5Cl and Li_6PS_5Br leads to ionic conductivities 3 orders of magnitude greater than

https://doi.org/10.1021/acs.chemmater.5c02939
Chem. Mater. 2026, 38, 3038−3058

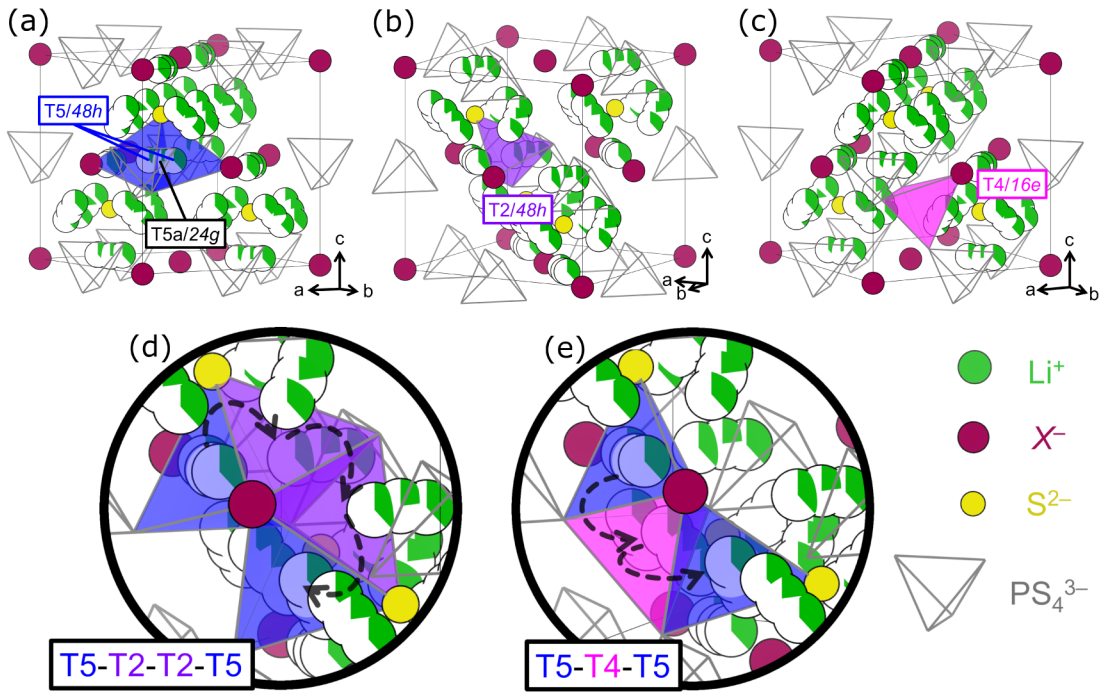

Figure 4. Tetrahedral voids and corresponding Li^+ sites that have been reported with significant occupation in the Li_6PS_5X ($X = Cl^-, Br^-, I^-$) system and its derivatives. The T5 and T5a sites (a) exhibit the highest occupancy and represent equilibrium positions. Population of the T2 (b) and T4 (c) sites is associated with fast ion conduction due to activation of T5-T2-T2-T5 (d) and T5-T4-T5 (e) intercage hopping pathways.

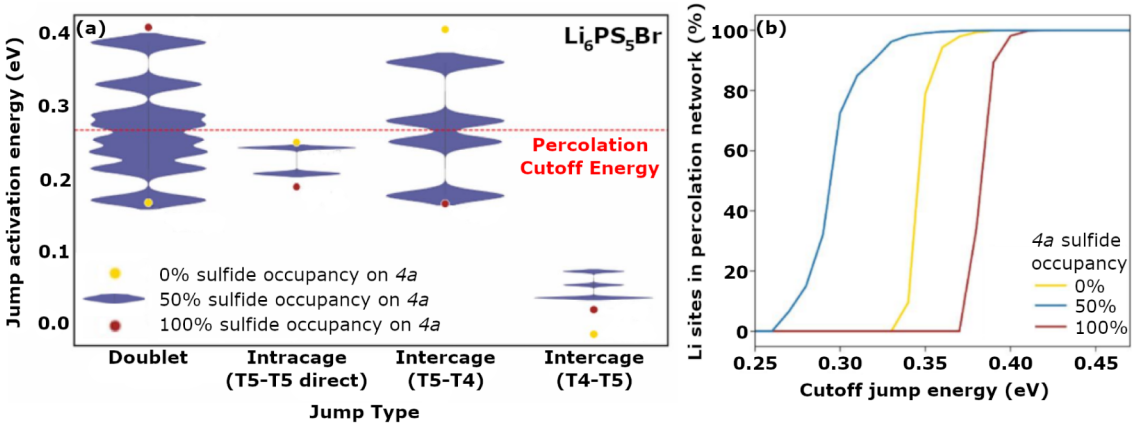

Figure 5. Local anion occupation on the 4*a* and 4*d* Wyckoff positions significantly influences the activation energies of doublet, intracage, and intercage transport pathways in Li_6PS_5Br (a). When anion site disorder is introduced, a variety of local environments are present (blue violin plots, width represents the relative prevalence of each local jump environment at 50% sulfide occupancy on 4*a*), which allow the formation of a percolating network at a lower cutoff energy than in either ordered configuration (b). Intracage hopping was treated as direct T5-T5 hopping, resulting in higher activation energies than those calculated for the T5-T2-T5 intracage pathway.[135] Activation energies associated with the T5-T2-T2-T5 follow the same trend as those for the T5-T4 intercage hops as a function of site disorder.[135] Adapted from ref 136. Copyright 2025 American Chemical Society.

Li_6PS_5I.[18,134] This increase in ionic conductivity arises from activation of the intercage T5-T2-T2-T5 and T5-T4-T5 hops needed for long-range ion conduction.[22] In anion-ordered systems, intercage pathways have large energy barriers. Mobile ions are confined to motions within the cages, resulting in low bulk ionic conductivity.[21,22,134−136] Figure 5 illustrates this behavior in Li_6PS_5Br.[136]

Anion antisite disorder enables the formation of percolating ion transport pathways by averaging the electrostatic charge of the anions and broadening the distribution of local electrostatic environments for Li^+. When S^{2-} exclusively resides on the 4*d* site (as in Li_6PS_5I), Li^+ remains localized in cages around the S^{2-} on the 4*d* site.[22] This favors the T5-T5 doublet hop, but strongly disfavors the T5-T4-T5 and T5-T2-T2-T5 hops needed for intercage transport (Figure 5a). When S^{2-} exclusively occupies the 4*a* site, the Li^+ cages form around that site, allowing low-energy T5-T2-T2-T5 and T5-T4-T5 hopping, but raising the activation barrier for the T5-T5 doublet hop. Introducing site disorder distorts the octahedral Li^+ cages and generates an ensemble of local environments with varying S^{2-} and X^- arrangements across 4*a* and 4*d* sites, which change the activation energies of nearby hopping pathways.[22] With sufficient site disorder, local environments that favor doublet hopping will have neighboring environments that favor intercage hopping (intracage hops are always accessible), allowing Li^+ to percolate through locally favorable environments with lowered activation

https://doi.org/10.1021/acs.chemmater.5c02939
Chem. Mater. 2026, 38, 3038−3058

barriers (Figure 5b).[22,135,136] We note that a broader distribution of electrostatic environments is more important for the formation of low-energy percolating pathways than simply lowering the charge density of the anion at the center of the Li^+ cages. This design principle is further supported by compositional derivatives of the argyrodite family. In multianion argyrodites such as $Li_{5.5}PS_{4.5}Cl_xBr_{1.5-x}$[137] and $Li_6PS_5(CN)_{1-x}Br_x$,[138] the additional disorder introduced by distributing all three anions across both the 4*a* and 4*d* sites results in lower average activation barriers and higher ionic conductivities relative to the single-(pseudo)halide analogs. Similarly, halide-enrichment in the $Li_{6-y}PS_{5-y}X_{1+y}$ (X = Cl^-, Br^-) argyrodites reduces the total average charge distributed across the 4*a*/4*d* sites and enforces anion site disorder, lowering the average activation barriers of the three hop types and converging them toward the same value.[27,28,35,53,135,136]

While it is convenient to discuss ion transport in the argyrodites as occurring via discrete hops along specific pathways, Figure 5 shows that anion disorder results in a broad distribution of energies associated with these pathways. Yet, temperature dependent ionic conductivity measurements yield single values for activation energy and Arrhenius prefactor. This seeming contradiction suggests that analysis of discrete hops, while conceptually useful, belies a regime characterized by highly correlated ion motion. The Haven ratio of 0.456 for Li_6PS_5Cl supports this notion.[124]

5. PHONONS

The dynamics of ion motion in solid-state ion conductors—particularly the coupling between lattice vibrations and mobile ions—are increasingly recognized as central to fast ion conduction. It is useful to consider these motions in terms of phonons: collective and coherent excitations of the lattice.[139,140] Reducing phonon frequencies results in an increased phonon population at a given temperature, and elevated phonon populations enable larger ion displacement amplitudes that facilitate ion hopping.[117,120,141,142] In this section, we examine the role of phonons in phase transitions and ion transport in the argyrodites.

5.1. Phase Transitions and Phonon "Melting"

The high-temperature aristotype of the argyrodites has long been understood to be a consequence of heavy disordering in the cation sublattice, which generates a high symmetry average structure.[33] In halide-free Ag^+ and Cu^+ argyrodites (e.g., Cu_7PSe_6[43,97] Cu_7PS_6[93] Ag_8GeSe_6[143] Ag_8SnSe_6,[29] the phase transition can be classified as an order−disorder transition in which the mobile ion sublattice "melts" while the anion sublattice remains relatively rigid. This "melting" is accompanied by a collapse of cation phonon modes into a heavily overdamped and anharmonic regime where these phonon frequencies approach zero energy and the oscillatory behavior of the system is suppressed. The breakdown of these phonons coincides with the onset of a dynamic regime in which the mobile ion sublattice exhibits liquid-like "superionic" transport.[29,43,93,97,139,143,144] In contrast, the anion sublattice remains largely ordered on average, with only minor modulations of the polyhedral units and free chalcogenides in the time-averaged structure (Figure 2).[93] Anharmonicity and phonon softening enable many argyrodites to exhibit ultralow lattice thermal conductivity relevant for applications in thermoelectrics.[29,43,97,145]

Cation "melting" is illustrated by the Ag_8SnSe_6 system, which exhibits a sharp phase transition from the low temperature $Pmn2_1$ structure to the high temperature $F\bar{4}3m$ structure at T = 355 K.[29] Concomitant with this phase transition, the inelastic neutron spectrum (INS) evolves from quasi-harmonic to quasi-elastic, overdamped behavior with increasing temperature (Figure 6a).[29] This evolution is consistent with Ag^+ ions

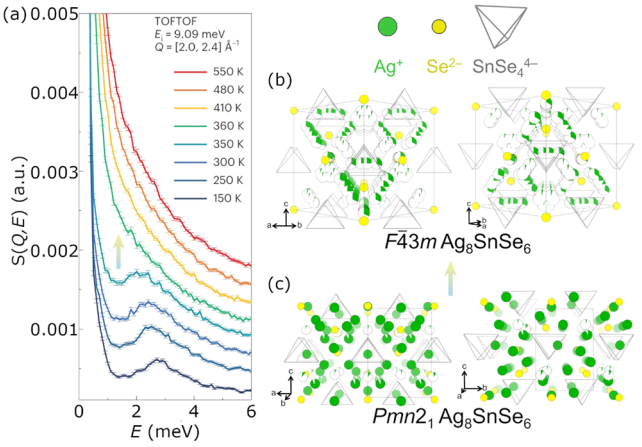

Figure 6. Ag_8SnSe_6 exhibits "melting" of Ag^+ sublattice reminiscent of a first order phase transition. This is characterized by the onset of a quasi-elastic component in the inelastic neutron spectrum (INS, integrated over a Q range of 2.0−2.4 Å^{-1}) between T = 350−360 K that is coincident with the phase transition at 355 K (a). From a structural perspective, this "melting" behavior can be seen in the change from an ordered Ag^+ sublattice in the low temperature $Pmn2_1$ structure (c) to a disordered Ag^+ sublattice in the high temperature $F\bar{4}3m$ structure (b). Panel (a) adapted with permission from ref 29. Copyright 2023 Springer Nature.

switching from oscillating about their equilibrium positions (quasi-harmonic) to rapid diffusion (quasi-elastic). The cation sublattice "melting" is captured in structural data through significant disordering of Ag^+ paired with only minor reordering of the anion sublattice (Figure 6b and c).

The above representation becomes more complex when multiple phase transitions are present over a narrow temperature range, as is the case for Ag_8GeSe_6 and Cu_7PSe_6.[43,97,143] Stepwise "melting" of the cation sublattice appears to occur, where each phase transition further disorders the cation sublattice. One possible explanation of this behavior is that the first hettotype-hettotype transition activates intracage ion diffusion (discussed in Section 4), while the hettotype-aristotype transition activates intercage ion diffusion and thereby allows long-range ion transport. Cu_7PSe_6 exhibits a transition from the low temperature $Pna2_1$ phase to the intermediate temperature $P2_13$ phase at T = 250 K.[97] Concomitant with this phase transition, localized oscillations of the Cu^+ sublattice give way to facile intracage ion transport and a quasi-elastic behavior appears in the INS (Figure 7a−c).[97] At T = 320 K, the $F\bar{4}3m$ structure is adopted and intercage transport is activated, at which point the cation melting transition is fully completed (Figure 7a,c,d).[97] The presence of multiple phase transitions in Cu_7PSe_6 has been attributed to the lower stability of d^{10} Cu^+ in low coordination number environments with Se^{2-}, which localizes Cu^+ ions in the low-temperature $Pna2_1$ structure.[76,146,147] In systems that undergo a single phase transition, such as Ag_8SnSe_6, both types of diffusion are activated simultaneously.

https://doi.org/10.1021/acs.chemmater.5c02939
Chem. Mater. 2026, 38, 3038−3058

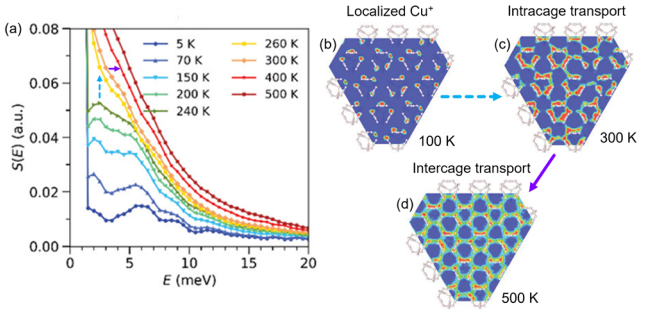

Figure 7. Cu_7PSe_6 exhibits phase transitions at 250 K and at 320 K that occur concomitant with cation sublattice "melting". (a) The inelastic neutron spectrum (INS) integrated over a Q range of 1−4 $Å^{-1}$ exhibits the onset of quasi-elastic behavior coincident with the 250 K transition (blue arrow). Cu^+ probability density maps of the (111) plane in the $F\bar{4}3m$ structure calculated from machine learned molecular dynamics simulations (b−d) show that this transition induces facile intracage transport (c). The phase transition to the $F\bar{4}3m$ structure at 320 K (purple arrow) allows for facile intercage hopping at elevated temperatures and completes the "melting" process (d). Adapted with permission from ref 97. Copyright 2022 John Wiley and Sons.

While halide-free Ag^+ and Cu^+ argyrodites both appear to exhibit "superionic" transitions characterized by cation sublattice melting, the halide argyrodites (e.g., A_6MCh_5X) appear to exhibit distinct phase transition behavior. Li_6PS_5Cl is only known to adopt the $F\bar{4}3m$ aristotypic structure down to 5 K, as determined by neutron powder diffraction.[148] Inelastic and quasielastic neutron scattering studies on $^7Li_6PS_5Cl$ indicate that the mobile ion sublattice exhibits progressive "melting" behavior from 50−600 K.[149] This behavior runs counter to the sharp cation sublattice "melting" transitions observed in halide-free Ag^+ and Cu^+ argyrodites and indicates that halide substitution fundamentally changes the behavior of the cation and polyhedral dynamics that participate in the phase transitions. Recent studies have found that the local structures of the Li_6PS_5X argyrodites are not well-described by the $F\bar{4}3m$ aristotype.[38,40] Rather, these deviations have been modeled by both supercell modulations and by pseudo-random rotational disorder of the PS_4^{3-} tetrahedra. Preservation of the $F\bar{4}3m$ aristotype to low temperatures combined with the local structure may suggest dynamic averaging of PS_4^{3-} dynamics, with higher temperatures resulting in higher-amplitude librations.

The onset of an overdamped, anharmonic regime calls into question the description of discrete hopping behavior discussed in Sections 3 and 4. Can cation transport in aristotypic argyrodites usefully be described as ions hopping between sites, or does absolute rate theory lose its validity? In many systems that are poorly described by absolute rate theory, transition to the superionic phase is accompanied by a discontinuous drop in E_A,[127] as is observed in the Cu^+ and Ag^+ superionic argyrodites.[43,145] In contrast, the lithium halide analogs appear to reside in the hopping regime at or near room temperature. Below T = 400 K, Li_6PS_5Cl exhibits a quadratic, Debye relationship between the vibrational density of states (VDOS) and phonon frequency ($g(\omega) \propto \omega^2$).[149] At T = 400 K, the INS develops quasi-elastic broadening characteristic of fast hopping or diffusion. At T = 600 K, the liquid-like regime is established, as evidenced by the linear relationship between VDOS and phonon frequency ($g(\omega) \propto \omega$). For Li_6PS_5Cl and the halide congeners, the liquid-like "superionic" regime is therefore not present at or near room temperature. As such, Arrhenius hopping and absolute rate theory are expected to be a valid framework for understanding ion transport at temperatures where ionic conductivities are typically measured experimentally.

5.2. Activation Energy (E_A)

The activation barrier for ionic conduction is strongly influenced by the phonons of the host lattice. The lowest energy optical phonon (LEO)—the lowest-frequency phonon where atoms move out of phase with one another—is important for ion transport as it plays a dominant role in displacing the mobile ion relative to the anions.[141] Early work by Wakamura established a correlation between the LEO phonon frequencies and activation energies across a variety of ion conductors, specifically in materials where mobile ion vibrational amplitudes exceed those of the framework ions.[141,150] Softening of these LEO modes and the corresponding reduction in activation energy are further linked to changes in the dielectric constants of ion conductors. As polarizability and dielectric constant increase, both activation energy and LEO phonon frequency tend to decrease.[141,151,152] This phonon-transport coupling arises from lattice softening effects—as the polarizability of constituent anions increases, more phonon modes become thermally accessible at a given temperature, leading to generally lower activation energies.[120,141,150] The physical basis for this relationship can be rationalized in the context of Pearson hard−soft acid−base theory: softer, more polarizable species can more effectively screen the electrostatic interactions with relatively hard cations, such as Li^+.[117,153] Thus, lattice softening creates shallower potential wells, and ions can access a wider portion of those wells at the same energetic cost, increasing the probability that a mobile ion will migrate into a neighboring stable site.

In Li_6PS_5X argyrodites, halide and chalcogenide substitution modify E_A for Li-ion transport through competing effects of lattice softening and anion site ordering. As shown in Figure 8, E_A decreases linearly with increasing Br^- content in $Li_6PS_5Cl_{1-x}Br_x$.[18] Similarly, Se^{2-} substitution in $Li_6PS_{5-x}Se_xI$ results in a monotonic decrease in E_A and yields a 2 orders of magnitude improvement in ionic conductivity.[110] Both of these

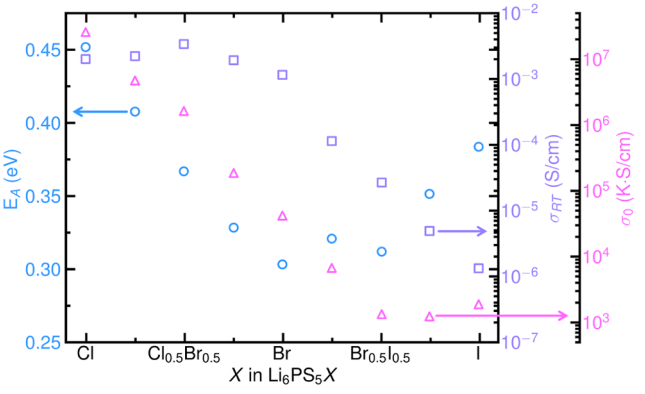

Figure 8. Activation energies (E_A, blue circles), Arrhenius prefactors (σ_0, pink triangles), and room temperature ionic conductivities (σ_{RT}, purple squares) for Li_6PS_5X (X = Cl^-, Br^-, I^-) and alloy compositions. E_A decreases with halide softening as Cl^- is replaced with Br^-, but upon introduction of I^-, E_A increases due to anion site ordering. σ_0 decreases with halide softening as Cl^- is replaced with Br^-. Further softening by addition of I^- continues to decrease σ_0 until the $Li_6PS_5Br_{0.5}I_{0.5}$ composition is reached. Additional I^- substitution exhibits a minimal effect on σ_0. Data reproduced from ref 18.

https://doi.org/10.1021/acs.chemmater.5c02939
Chem. Mater. 2026, 38, 3038−3058

cases are consistent with the general principle that increasing lattice polarizability lowers E_A. This general rule can be weaker than structure effects, specifically anion ordering. Based on polarizability, substitution of Br^- with I^- would be expected to decrease E_A. In practice, introducing I^- leads to ordering of S^{2-} and X^- anions on the 4*d* and 4*a* sites concurrent with an increase in E_A.[18] Anion ordering also occurs in $Li_6PS_{5-x}Se_xBr$, where addition of Se^{2-} results in a slight increase in both E_A and ionic conductivity.[154] Full ordering of the anion species increases E_A for the rate limiting intercage hop and generally exerts a stronger influence than anion polarizability, as detailed in Section 4.[18,20−23] In light of these case studies, both site disorder and anion polarizability exert strong influences on E_A in Li_6PS_5X argyrodites.

5.3. Arrhenius Prefactor (σ_0)

Until recently, E_A has dominated discussions of ion conduction, while the prefactor (σ_0)—which contains terms with significant influence on ionic transport—has often been neglected. As shown in eq 2, σ_0 is a collection of temperature-independent terms and is determined via temperature-dependent ionic conductivity measurements.

In Li_6PS_5X (X = Cl^-, Br^-, I^-), several terms in the prefactor remain relatively constant. γ and Ze remain unchanged due to fixed pathway dimensionality and ion charge. The lattice parameter varies by only ≈ 3% from Li_6PS_5Cl to Li_6PS_5I,[18] so changes in a_0 and c—which is not expected to change significantly with constant Li^+ content—cannot account for the observed 3 orders of magnitude difference in σ_{RT}. Tuning Li^+ content through aliovalent substitution of P^{5+} or by varying the S^{2-}/X^- ratio is expected to impact c, but we focus this section on materials with fixed Li^+ content.[20,25,28,35,53] For Li_6PS_5X (X = Cl^-, Br^-, I^-), ν_0 and ΔS_m are primary drivers for variation in σ_0 and are intimately connected to dynamics. ν_0 is the frequency that the mobile ion attempts a hop and is generally accepted to be synonymous with the frequency at which the mobile ion oscillates about its equilibrium position.[119] If a mobile ion oscillates at a higher frequency and makes more hopping attempts with a fixed probability of success, it will succeed more often and the ionic conductivity will increase.

The Debye frequency (ν_D) is generally accepted to be a reasonable approximation of attempt frequency in absolute rate theory.[112] ν_D is the cutoff frequency in the Debye model that approximates the maximum frequency of acoustic phonon modes in the crystal.[155] The Debye temperature, θ_D, is defined as $\theta_D \equiv h\nu_D k_B^{-1}$ and corresponds to the temperature at which all normal modes are thermally accessible.[155] Physically, ν_D corresponds to the frequency at which the phonon wavelength is on the order of the unit cell dimensions and represents the shortest wavelength consistent with the crystal periodicity.[156] If the speed of sound within a structure is assumed constant for all frequencies, ν_D can be calculated according to:

$$\nu_D = \left(\frac{3}{4\pi V}\right)^{1/3} v \tag{5}$$

where V is the volume of the unit cell and v is the speed of sound through the material.[18,155,156]

ΔS_m appears to be a stronger driver of the magnitude of the Arrhenius prefactor in argyrodites than ν_D. Speed of sound measurements of the $Li_6PS_5Cl_{1-x}Br_x$, $Li_6PS_5Br_{1-x}I_x$, and $Li_6PS_{5-y}Se_yI$ compositional series reveal the general trend that the introduction of larger and more polarizable anions reduces the magnitude of the ν_D. For $Li_6PS_5Cl_{1-x}Br_x$ and $Li_6PS_{5-y}Se_yI$, ν_D decreases monotonically and mirrors the trends in E_A (Figures 8 and 9a), supporting the case that lattice polarizability lowers E_A.[18,110] ν_D alone is insufficient to explain trends in σ_0; σ_0 is expected to scale linearly with ν_0 (approximated by ν_D), but this is not observed in either Li_6PS_5X or $Li_6PS_{5-y}Se_yI$. In Li_6PS_5X, ν_D varies by only ~25% and σ_0 spans 4 orders of magnitude, indicating that ν_0 is not the primary driver of σ_0 values.[18] Similarly, ν_D varies by a factor of 2 in $Li_6PS_{5-y}Se_yI$ (Figure 9c), while σ_0 varies by a full order of magnitude.[110] As such, the linear relationship between ν_0 and σ_0 ($\sigma_0 \propto \nu_0$) is insufficient to explain trends in σ_0. Instead, σ_0 appears to be exponentially correlated with halide occupancy on the 4*d* site ($\sigma_0 \propto e^{disorder}$, Figure 9b and d). This relationship mirrors the dependence of σ_0 on ΔS_m ($\sigma_0 \propto e^{\Delta S_m}$) and implies that halide occupancy on the 4*d* site generates a broadened distribution of vibrational environments, which increases ΔS_m and drives large changes in σ_0. Confirmation of this dependence requires calculating or estimating ΔS_m.

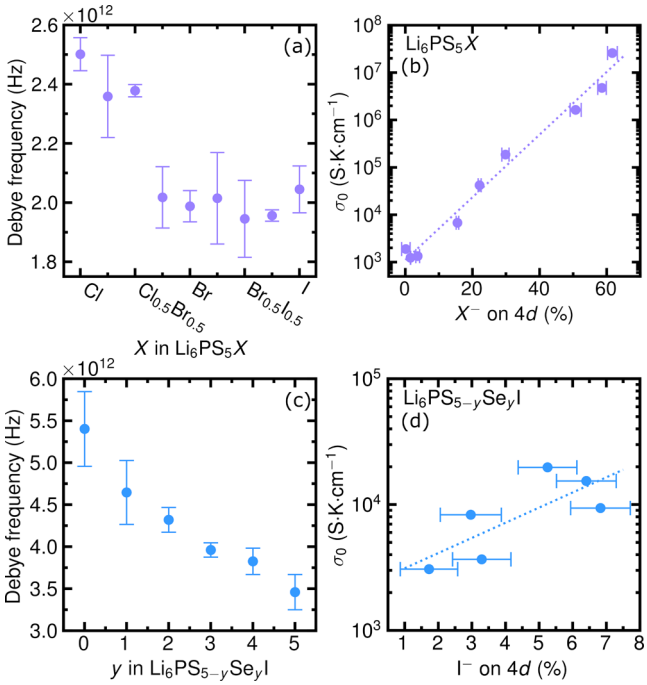

Figure 9. Debye frequencies (ν_D) are reduced with increasing halide (a) and chalcogenide (c) polarizability. Arrhenius prefactors (σ_0) trend exponentially with halide occupancy on the 4*d* Wyckoff position (b, d). Dotted lines in (b) and (d) are guides to the eye. Data reproduced from ref [18,110].

A method of calculating ΔS_m is emerging in the solid-state ionics literature. This method relies on reframing the Arrhenius relationship in eq 1 from terms of ionic conductivity to hopping frequency, thereby eliminating most of the linear terms in the prefactor.[27,138,157,158] This allows for calculation of ΔS_m given hopping frequency, ΔH_m, and attempt frequency. Hopping frequency can be obtained from the characteristic frequency of the equivalent circuit element representing bulk ion transport in EIS.[27,157] ΔH_m can then be determined via the Arrhenius relationship, as is commonly done for E_A. Finally, attempt frequency can be estimated using ν_D or MD simulations.[27,138,157] In the argyrodites, ΔS_m values were recently calculated for $Li_{6-x}PS_{5-x}Br_{1-x}$ via the characteristic frequency approach and ΔS_m was found to positively correlate with Br^- occupation on

https://doi.org/10.1021/acs.chemmater.5c02939
Chem. Mater. 2026, 38, 3038−3058

the 4*d* site.[27] This supports the hypothesis that changes in σ_0 in Li_6PS_5X are driven by changes in ΔS_m that are induced by site disorder, as σ_0 scales exponentially with site disorder in Li_6PS_5X alloys (Figure 8).[18] As an alternative to the hopping frequency method, ΔS_m was approximated using σ_0, ν_D as attempt frequency, and a range of carrier concentrations and jump distances in $Li_6PS_5(CN)_{1-x}Br_x$.[138] Validation and routine adoption of these methods would clarify the extent to which ΔS_m or the linear terms drive changes in σ_0.

5.4. The Meyer-Neldel "Compensation" Regime

Just as E_A is generally reduced by softening of the vibrational landscape, σ_0 is often simultaneously decreased. As discussed above, several terms in σ_0 remain approximately constant within a material family and the bulk of the changes in σ_0 can be attributed to ΔS_m.[120] In this context, the simultaneous increase or decrease in E_A and σ_0 arises from enthalpy−entropy compensation. From the perspective of multiexcitation entropy theory, increasing the height of the activation barrier (E_A) means that there are more possible ways to reach the excited state, driving ΔS_m and σ_0 higher.[120] This phenomenon is commonly referred to as the Meyer-Neldel compensation rule.[159] Breaking the Meyer-Neldel compensation rule, or finding materials that follow the so-called anti Meyer-Neldel rule,[160] is therefore an exciting prospect for achieving high ionic conductivities.

In Li_6PS_5X ($X = Cl^-, Br^-, I^-$), the Cl^-/Br^- alloy series is firmly in a "compensation regime", where changes in E_A and σ_0 largely cancel one another and ionic conductivity changes very little.[18] This compensatory behavior is evident when σ_0 is plotted against E_A (Figure 10), where a linear relationship with positive slope on a logarithmic scale is observed for the Cl^-/Br^- alloy series.[18] Notably, the I^-/Br^- alloy series does not reside in this regime and can be considered to "break" Meyer-Neldel behavior (Figure 10). Rather, substituting I^- with Br^- leads to a concurrent decrease in E_A and increase in σ_0. This results in a three-order-of-magnitude increase in room-temperature ionic conductivity across the alloy series, which is attributed to the introduction of anion site disorder.[18]

Indeed, a variety of argyrodite compositions that do not fall into the compensation regime have been reported (Figure 11). This group of noncompensatory argyrodites is dominated by $Li_{6+x}P_{1-x}M_xS_5I$, where M is a tetravalent cation. As with Br^- substitution in $Li_6PS_5I_{1-x}Br_x$, M^{4+} substitution in $Li_{6+x}P_{1-x}M_xS_5I$ commonly induces S^{2-}/I^- site mixing, indicating that inducing anion site disorder in anion-ordered argyrodites is an effective approach for inducing noncompensatory behavior.[20,161] To clarify this design principle: compensatory behavior is expected when site disorder is either present across an entire compositional series or absent across the entire series. In contrast, noncompensatory behavior emerges when site disorder is introduced partway through an alloy series (i.e., when one end member is ordered but intermediate compositions or the opposite end member exhibit disorder). While the loss of site disorder disrupts Meyer-Neldel behavior by localizing the divalent sulfide anion on the 4*d* site, incorporation of high charge density pseudohalides on the 4*d* site produces a similar result. In $Li_6PS_5(CN)_{1-x}Br_x$, high charge density CN^- on the 4*d* site is linked to increased ΔS_m according to eq 3, disrupting Meyer-Neldel behavior.[138] In these noncompensatory cases, the electrostatics of the 4*d* site play a decisive role in ΔS_m. Further discussion of the mechanisms behind this noncompensatory behavior can be found in Section 6. In general, very high ionic conductivities are achieved in soft, polarizable host frameworks that enable anion antisite disorder.

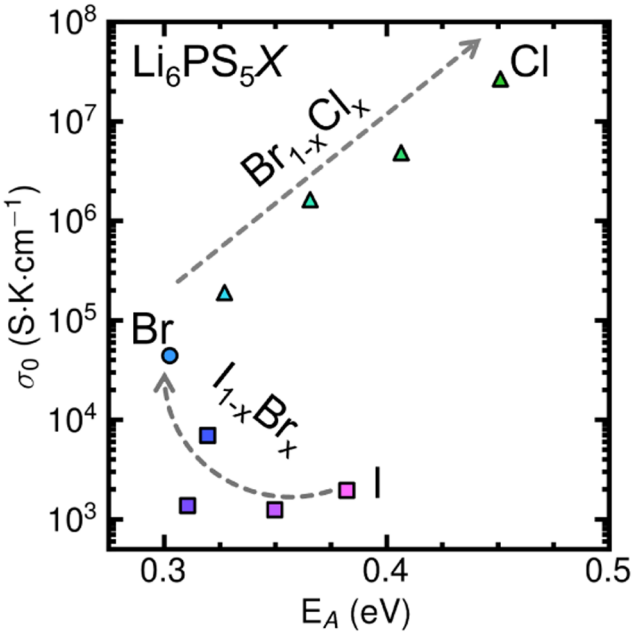

Figure 10. Arrhenius prefactor (σ_0) plotted against activation energy (E_A) for Li_6PS_5X ($X = Cl^-, Br^-, I^-$) and alloys of mixed halides. The introduction of S^{2-}/X^- site disorder in the $Li_6PS_5I_{1-x}Br_x$ alloy series (pink to blue, squares) causes a simultaneous decrease in activation energy and increase in prefactor, which breaks the Meyer-Neldel rule. Once sufficient disorder is achieved in Li_6PS_5Br, the Meyer-Neldel rule holds. This trend is observable in the $Li_6PS_5Br_{1-x}Cl_x$ alloy series (blue to green, triangles). Li_6PS_5Br is indicated with a circle as it represents an end member of both alloy series. Gray dashed arrows are guides to the eye indicating the two alloy series and do not represent fits to the data. Data reproduced from ref 18.

6. LOCAL POLYANION DYNAMICS

Argyrodites are amenable to local dynamics of polyhedral and molecular species. In this section, we highlight the known studies of dynamics of the MCh_4 tetrahedral units as well as the dynamics of molecular "pseudohalide" anions and discuss compositional and structural origins that dictate the presence, timescales, and amplitudes of these dynamics. Given the presence of these dynamics, we then discuss potential mechanisms for coupling between polyanion motion and Li^+ diffusion.

6.1. Polyhedral Dynamics

The structurally isolated MCh_4 units can undergo dynamics, and the timescales of these motions are sensitive to the surrounding environment. ^{31}P spin lattice relaxation nuclear magnetic resonance (SLR NMR) studies have recently provided extensive insights into PS_4^{3-} dynamics in the lithium halide argyrodites (Table 2).

Early studies found that the identity of the halide anion strongly correlates with the timescales of PS_4^{3-} dynamics. Across the series $Li_6PS_5Cl \rightarrow Li_6PS_5Br \rightarrow Li_6PS_5I$, introducing larger and more polarizable halides results in a progressive increase in the rotation rates of the PS_4^{3-} tetrahedra (Figure 12).[49] Li_6PS_5Br and Li_6PS_5I both exhibit two distinct types of relaxation processes, which have been assigned to PS_4^{3-} dynamics (low T

https://doi.org/10.1021/acs.chemmater.5c02939
Chem. Mater. 2026, 38, 3038−3058

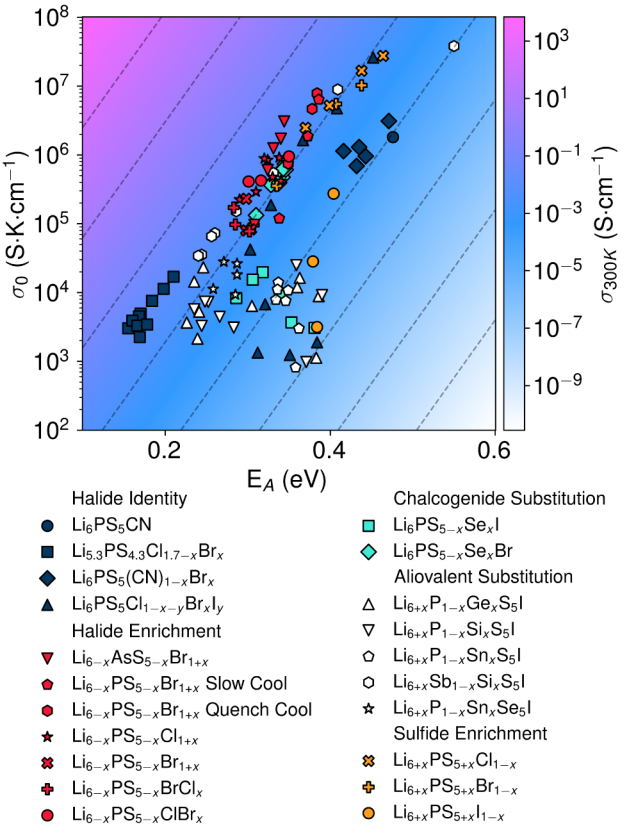

Figure 11. Arrhenius prefactor (σ_0) plotted against activation energy (E_A) for a selection of lithium argyrodites. The color gradient represents ionic conductivity at T = 300 K and the dashed lines represent contours of constant ionic conductivity. Where necessary, σ_0 was calculated from room temperature ionic conductivity and activation energy according to the Arrhenius relationship with room temperature assumed to be 298 K. Data reproduced from ref [18,20,25,27,28,34−36,50,53,54,108,110,138,154,161].

peak) and relaxation due to the transit of nearby Li^+ spins (high T peak).[49,131] In Li_6PS_5Cl, only a single feature is observed, indicating that both relaxation processes are occurring on similar time scales. In SLR NMR, the probed rate is fixed by the Larmor frequency (ω_0) of the probed nucleus and temperature is varied; when a peak in $\log(1/T_1)$ versus $1/T$ is observed, the correlation rate of the observed process ($1/\tau_{rot}$) is equal to $2\pi \times \omega_0$. Rate peaks corresponding to PS_4^{3-} rotations occurring at $\sim 10^9$ s^{-1} (ω_0 = 121 MHz) are observed at T = 283, 233, and 223 K for Li_6PS_5Cl, Li_6PS_5Br, and Li_6PS_5I, respectively (Table 2).[49] The systematic shift of the rate peak to lower temperatures is indicative of faster PS_4^{3-} rotational dynamics.

In the same way that anion antisite disorder strongly impacts lithium ion dynamics (Section 4), anion disorder also impacts the timescales of tetrahedral rotations. A ^{31}P SLR study of the halide series $Li_{5.3}PS_{4.3}Cl_{1.7-x}Br_x$ series demonstrated that Li^+ and PS_4^{3-} exhibit similar motional rates in heavily halide-enriched compositions, just as in Li_6PS_5Cl.[36,49] Increasing bromide content leads to faster timescales of PS_4^{3-} dynamics, but does not impact rotation rates sufficiently to yield distinct timescales for PS_4^{3-} and Li^+ motions.[36] Mixed-halide members of the halide-rich compositional series appear to exhibit faster PS_4^{3-} dynamics than either of the end-members. Faster tetrahedral dynamics were also observed when the local anion configuration favored Cl^-, Br^-, and S^{2-} site sharing on the 4d site compared to when the 4d site was occupied by S^{2-} and one halide species.[36] Taken together, these observations suggest that anion site disorder creates a broader variety of local environments experienced by the tetrahedral units, and that reducing the average anion charge and charge density of the 4d site enables faster tetrahedral rotations. Notably, changes in rotation rate for the $Li_{5.3}PS_{4.3}Cl_{1.7-x}Br_x$ series were not reported to cause PS_4^{3-} and Li^+ motions to occur on differing time scales, indicating that

Table 2. Time Constants (τ_0, s) and Activation Energies (E_A, eV) for PS_4^{3-} and Li^+ Motion for Several Lithium Halide Argyrodites, as Determined by ^{31}P and ^{7}Li Spin-Lattice Relaxation Solid-State NMR Studies in the Laboratory Frame[a]

Compound	^{31}P τ_0 (s)	^{7}Li τ_0 (s)	^{31}P E_A (eV)	^{7}Li E_A (eV)	T_{max} (K)	Note	Reference(s)
Li_6PS_5Cl	5.00×10^{-13}	1.30×10^{-14}	0.18	0.32	283	^{31}P peak due to PS_4^{3-} rotations and nearby Li^+ diffusion	49
Li_6PS_5Br	9.09×10^{-13}	2.27×10^{-14}	0.15	0.21	233	^{31}P low T peak due to PS_4^{3-} rotations	49
Li_6PS_5Br	9.09×10^{-12}	2.27×10^{-14}	0.14	0.21	–	^{31}P high T peak due to nearby Li^+ diffusion	49
Li_6PS_5I	5.55×10^{-14}	8.33×10^{-13}	0.2	0.2	223	^{31}P low T peak due to PS_4^{3-} rotations	49
Li_6PS_5I	3.45×10^{-11}	8.33×10^{-13}	0.18	0.2	–	^{31}P high T peak due to nearby Li^+ diffusion	49
Li_6PS_5I	3.45×10^{-12}	8.33×10^{-13}	0.18	0.2	–	Peak 1; translational, fast Li^+ intracage dynamics	131
Li_6PS_5I	5.00×10^{-12}	3.33×10^{-13}	0.44	0.26	–	Peak 2; translational, fast Li^+ exchange between cages	131
Li_6PS_5I	5.55×10^{-14}	–	0.2	–	220	Peak 3; rotational jumps of the polyanions	131
Li_6PS_5I	$4(3) \times 10^{-12}$	$0.8(1) \times 10^{-12}$	0.44(4)	0.18(1)	219		24
$Li_{6.1}P_{0.9}Ge_{0.1}S_5I$	$7(3) \times 10^{-11}$	$1.5(8) \times 10^{-12}$	0.29(2)	0.119(3)	230		24
$Li_{6.3}P_{0.7}Ge_{0.3}S_5I$	$4(1) \times 10^{-9}$	$4(2) \times 10^{-12}$	0.17(1)	0.098(1)	236		24
$Li_{6.6}P_{0.4}Ge_{0.6}S_5I$	$7(4) \times 10^{-10}$	$0.8(5) \times 10^{-12}$	0.13(1)	0.119(4)	253		24

[a] T_{max} corresponds to the temperature at which the rotational correlation rate ($1/\tau_{rot}$) for PS_4^{3-} rotations is $\sim 10^9$ s^{-1} as determined by the rate peak of ^{31}P SLR measurements (Larmor frequency of 121 MHz).

https://doi.org/10.1021/acs.chemmater.5c02939
Chem. Mater. 2026, 38, 3038−3058

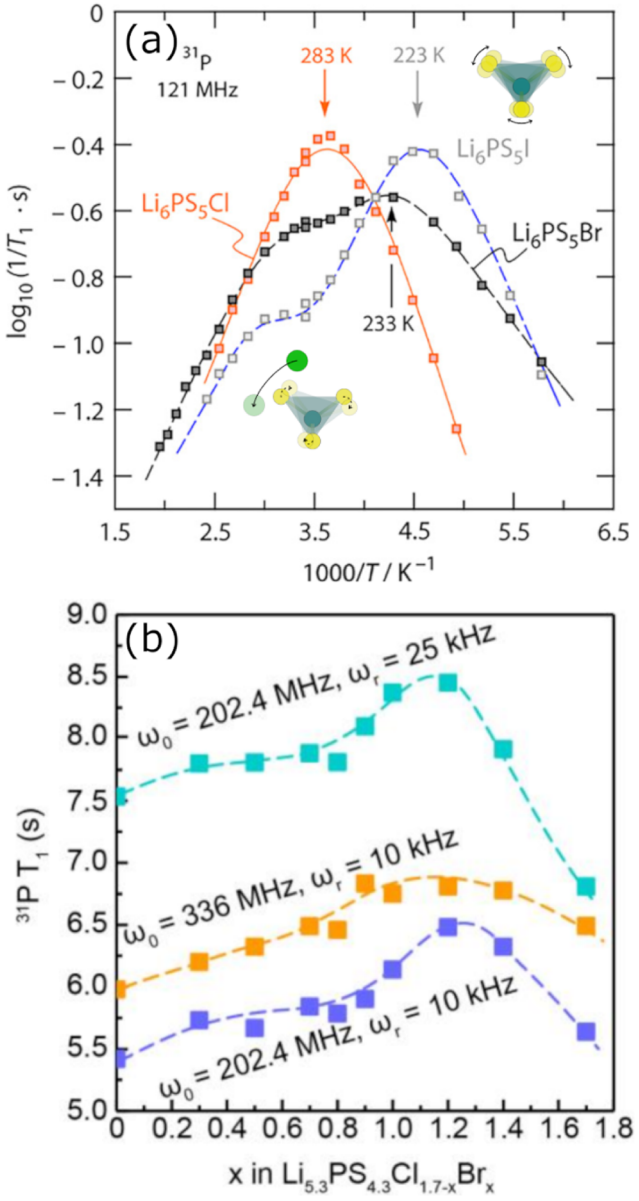

Figure 12. (a) ^{31}P spin−lattice relaxation nuclear magnetic resonance (SLR NMR) provides insight into PS_4^{3-} rotational dynamics. In Li_6PS_5I and Li_6PS_5Br, the lower temperature rate peaks are attributed to PS_4^{3-} rotations (right inset), while the higher temperature shoulders are associated with Li^+ hopping sensed by ^{31}P spins (left inset). Peaks at lower temperatures correspond to faster processes. The two features cannot be distinguished in Li_6PS_5Cl, which indicates that the two processes occur at comparable rates. (b) PS_4^{3-} tetrahedra exhibit faster dynamics for mixed halide compositions, due to the extensive anion site disorder that creates a distribution of local environments for the tetrahedral units. (a) adapted and (b) reproduced with permission from ref 49 and ref 36. Copyrights 2019 American Chemical Society and 2023 John Wiley and Sons, respectively.

the impacts of site disorder and halide identity in the very halide-rich regime are small in comparison to those observed from $Li_6PS_5Cl \rightarrow Li_6PS_5Br \rightarrow Li_6PS_5I$.[36,49]

The timescales of tetrahedral dynamics are also sensitive to cation substitution effects at the center of the tetrahedra. Ge^{4+} substitution in the $Li_{6+x}P_{1-x}Ge_{0.1}S_5I$ series is accompanied by slowing of the PS_4^{3-} dynamics.[24] This may be due to differences in cation radii (r_P = 0.17 Å, r_{Ge} = 0.39 Å),[162] introduction of anion site disorder, or the larger average anion charge of the GeS_4^{4-} tetrahedra that modify the environment in the vicinity of the PS_4^{3-} units. ^{31}P relaxometry measurements are selective for the phosphorus nuclei, and thus the dynamics of the GeS_4^{4-} tetrahedra remain an open question. As ^{31}P relaxometry studies of cation-substituted argyrodites are sparse, further studies are needed to establish how the composition of the tetrahedra impacts their dynamics.

Signatures of (dynamic) rotational disorder of the isolated tetrahedral units have been observed through static, local structure probes. As early as 2017, experimental pair distribution functions (PDF) of Li_6PS_5X (X = Cl^-, Br^-, I^-) revealed inconsistencies between the local structure and the $F\bar{4}3m$ average structure observed by Bragg diffraction.[18] Modeling methods that capture this disorder have recently enabled quantification of the spatial extent of tetrahedral dynamics in the argyrodites.[38,40] Recently, we employed a rigid-body modeling routine in which the PS_4^{3-} units were allowed to rotate freely.[38] The resulting supercell exhibits pseudorandom rotations of the PS_4^{3-} away from their equilibrium positions by angles of ∼20−30° (Figures 13 and 14). By quantifying the distribution of

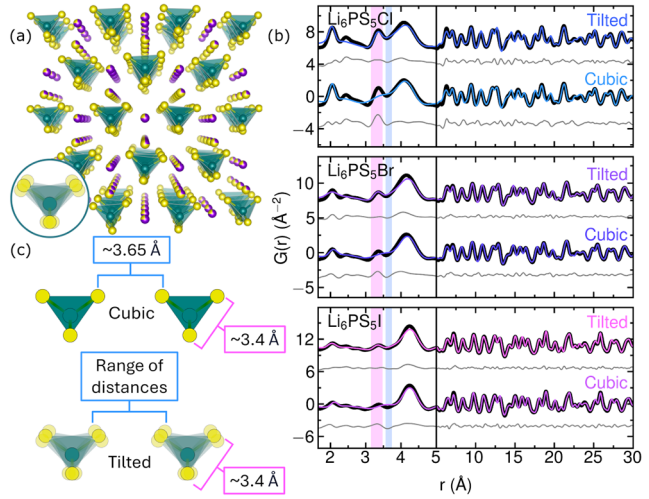

Figure 13. Dynamic tilting of the PS_4^{3-} tetrahedra (a) in Li_6PS_5X (X = Cl^-, Br^-, I^-) leads to discrepancies between the local and average structures (b).[38] As illustrated in (b), fitting with the cubic $F\bar{4}3m$ average structural model results in undermodelling of the intra-PS_4^{3-} S-S pair correlation (∼3.4 Å, pink vertical bar) and overmodelling of the inter-PS_4^{3-} S-S pair correlation (∼3.65 Å, blue vertical bar). Allowing PS_4^{3-} units to rotate as rigid bodies results in a range of inter-PS_4^{3-} S-S distances and improves fitting of the highlighted pair correlations. This behavior is shown in (c), where the pink callouts correspond to the intra-PS_4^{3-} S-S distances and the blue callouts correspond to the inter-PS_4^{3-} S-S distances. Data reproduced from ref 38.

displacements relative to the cubic structure, we found that the amplitude of the rotations increase across the Li_6PS_5I < Li_6PS_5Br < Li_6PS_5Cl series and are strongly correlated with site disorder (Figure 14). Given this local structure information and the aforementioned NMR studies, PS_4^{3-} rotation rates appear to be inversely correlated with rotation amplitude and 4*a*/4*d* site mixing; Li_6PS_5I exhibits the fastest and smallest rotations, whereas Li_6PS_5Cl exhibits the slowest and largest. Notably, the

https://doi.org/10.1021/acs.chemmater.5c02939
Chem. Mater. 2026, 38, 3038−3058

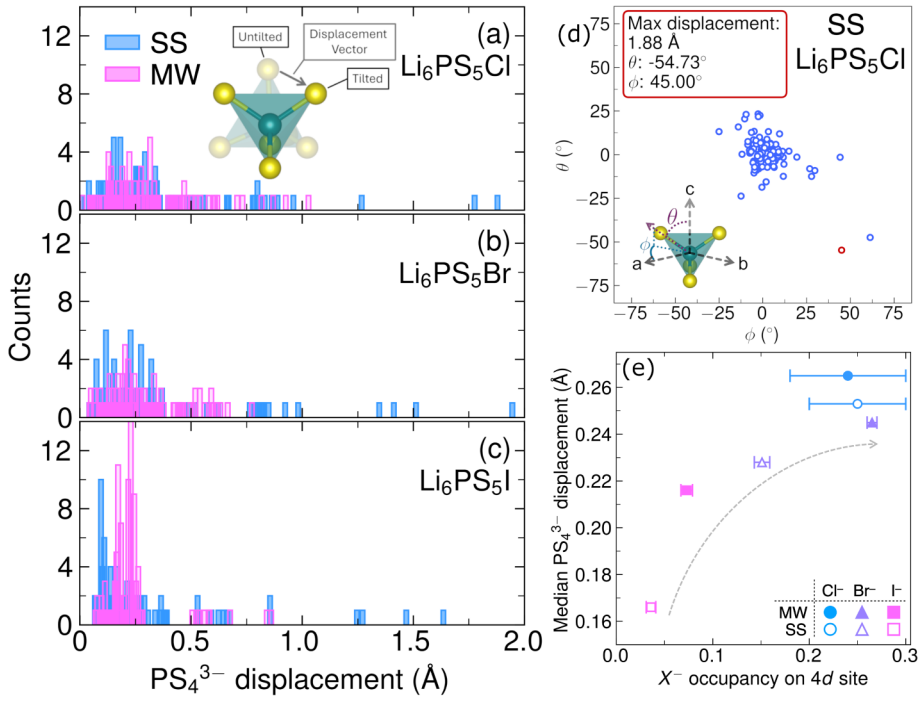

Figure 14. Rotational displacements of PS_4^{3-} units are correlated with halide identity, synthesis method, and S^{2-}/X^- site mixing. Panels (a), (b), and (c) show histograms of polyhedral rotational displacement as a function of synthesis method. SS corresponds to materials prepared by traditional solid-state synthesis and MW corresponds to materials prepared by rapid microwave synthesis method. The directionality and magnitude of polyhedral displacements is pseudorandom and clustered about the PS_4^{3-} orientation in the $F\bar{4}3m$ aristotype (d). PS_4^{3-} displacement is positively correlated with S^{2-}/X^- site mixing (e). Adapted with permission from ref 38. Copyright 2025 John Wiley and Sons.

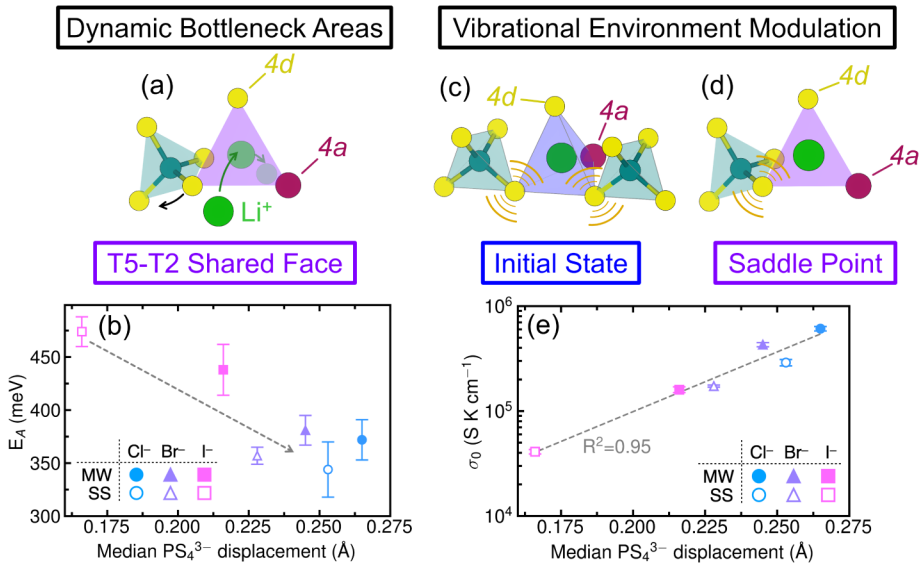

Figure 15. T5-T2 shared face represents a likely bottleneck for ion conduction in Li_6PS_5X argyrodites. It is defined by a 4*d* site, a 4*a* site, and one bonded tetrahedral sulfur. Polyhedral librations dynamically change the bottleneck area (a), facilitating Li^+ hops through the bottleneck. (b) illustrates the resulting dependence of E_A on polyhedral displacement. Changes in polyhedral rotational behavior disproportionately impact the vibrational environment about the initial state (c) and the saddle point (d). This results in a strong dependence of σ_0 upon polyhedral displacement, as shown in (e). Filled symbols (MW) correspond to argyrodites synthesized via a dry microwave method, while open symbols (SS) represent materials made via a conventional solid-state route. Polyhedral displacement is defined as the distance between a bound sulfur in the $F\bar{4}3m$ structure and the position of that sulfur in the rotationally disordered structure. Note that the T5-T2 hop is assumed to be rate limiting for the purposes of this figure, although the T2-T2 and T5-T4 hops may also represent rate limiting steps for intercage hopping. Panels (b) and (e) adapted with permission from ref 38. Copyright 2025 John Wiley and Sons.

neutron PDF of $Li_6PS_{4.5}Se_{0.5}Br$ reveals similar signatures of tetrahedral rotational disorder; however, the deviations appear to be significantly less with Se^{2-} than with S^{2-}. This observation suggests that the larger Se^{2-} anion modifies the amplitudes and timescales of polyhedral rotations.[154]

https://doi.org/10.1021/acs.chemmater.5c02939
Chem. Mater. 2026, 38, 3038−3058

The lithium ion transport properties of the Li_6PS_5X (X = Cl^-, Br^-, I^-) argyrodites are correlated with the amplitude and timescales of tetrahedral dynamics. As shown in Figure 15, higher median amplitudes of the PS_4^{3-} rotations determined by X-ray PDF (XPDF) are correlated with lower activation barriers (E_A), larger Arrhenius prefactors (σ_0) and generally higher ionic conductivities (σ). Lower activation energies track with both the degree of site disorder and higher amplitudes of tetrahedral rotations. As discussed in Section 4, anion site disorder creates a broader distribution of low-energy pathways for Li^+, which contribute to lower activation energies for macroscopic transport (Figure 5).[135] Larger-amplitude displacements of the PS_4^{3-} are expected to further contribute to this effect by creating dynamically fluctuating bottleneck areas for mobile ions. Expanding the bottleneck area through which ions must pass generally decreases E_A by reducing the electrostatic interactions between the mobile ion and the anion sublattice.[117,163−165] This phenomenon is often interpreted through a static structural picture,[20,110,154,161] but polyanion rotations[47,166−168] and translations[97] as well as "dynamic breathing" of the lattice[149] are known to transiently change bottlenecks and facilitate ion transport. The exponential increase in σ_0 with increasing polyhedral displacement amplitudes suggests that the dynamics of the tetrahedra modify the vibrational properties surrounding mobile ion sites. Assuming quasi-random librations of all polyhedra in the argyrodite structure, changes in oscillation rate and amplitude disproportionately affect the vibrational environments of the stable sites (T5, T5a) and the saddle points (T5-T2, T2-T2, and T5-T4 shared faces) relevant to ion conduction. These sites are vibrationally distinct because their geometric relationships to the tetrahedral units differ (Figure 15c and d). Consequently, modifications to the overall oscillatory behavior of the polyhedra alter the vibrational partition functions of the initial state and saddle point, increasing ΔS_m (eq 3) and, in turn, σ_0 (Figure 15e).

The presence of dynamic polyhedral rotations holds additional implications for the phase transition behavior observed in the argyrodites. Order−disorder transitions in materials with dynamic polyhedral rotations are often driven by softening and eventual freezing out of rotary modes with decreasing temperature.[169,170] A recent PDF study in Ag_8GeS_6, Ag_9GaSe_6, and Ag_8GeTe_6 argyrodites revealed that the low-r pair correlations of the high temperature aristotype were better modeled by a hettotype structure, indicating that disordering occurs concurrent with the phase transition.[39] Therefore, we hypothesize that activation of libratory modes—likely through dynamic sampling of local hettotype configurations—drives order−disorder phase transitions in argyrodites. As discussed in Sections 5 and 2, the phase transitions are accompanied by significant disordering of the mobile ion sublattice, which may be further impacted by the onset of polyhedral dynamics.[29,33,39] A closely related phenomenon is observed in Na_3PS_4, where the $\alpha \rightarrow \beta$ phase transition is accompanied by activation of PS_4^{3-} dynamics that facilitate fast ion transport.[41] In both Na_3PS_4 and the substituted analog $Na_{3-x}Sb_{1-x}W_xS_4$, the XPDF of the high-temperature phase retains signatures of the lower-symmetry hettotype characterized by tilted MS_4 tetrahedra.[41,42,171] Taken together, evidence from the argyrodites and the Na_3PS_4 structural family points toward a common mechanistic motif: order−disorder phase transitions characterized by activation of polyhedral dynamics that simultaneously promote fast ion transport.

6.2. Molecular Moieties

Beyond PS_4^{3-} units, the polyatomic pseudohalides BH_4^- and CN^- can be substituted at the halide position(s) in Li_6PS_5X.[105,107,108,138,172] Substituting molecular species at these sites introduces new rotational and vibrational dynamics into the argyrodite framework.

Incorporation of tetrahedral BH_4^- in $Li_6PS_5BH_4$ represents one approach to add additional polyhedral anions to the lattice, but synthesizing the target phase has proven challenging. Formation of the argyrodite phase requires $LiBH_4$-rich precursors.[105,106] This stems from the thermal instability of $LiBH_4$, which decomposes at typical synthesis temperatures for Li_6PS_5X; reliable reports of $Li_6PS_5BH_4$ are therefore scarce.[173] Nevertheless, $Li_6PS_5BH_4$ is reported to exhibit higher ionic conductivity than both Li_6PS_5Cl and Li_6PS_5Br.[105] Computational studies disagree on the atomistic origin of this enhancement: some report that BH_4^- rotates responsively to Li^+ hops and thereby facilitates diffusion,[172] whereas others suggest that weak Li-H interactions, rather than BH_4^- reorientation, are responsible.[105] The possibility of coupled rotational dynamics between PS_4^{3-} and BH_4^- remains largely unexplored. We note that H^+ conduction may be nontrivial due to incorporation of H^+ liberated from excess $LiBH_4$, but this has not been thoroughly investigated.[105,172,173] If H^+ is present and mobile in as-prepared $Li_6PS_5BH_4$, the elevated ionic conductivity observed in $Li_6PS_5BH_4$ could be an outgrowth of H^+ transport rather than enhanced Li^+ conduction.

Li_6PS_5CN represents an interesting case due to its dipolar pseudohalide—where both PS_4^{3-} and BH_4^- are tetrahedral, CN^- adopts a linear geometry. As such, the arrangement of CN^- ions in Li_6PS_5CN exhibits a strong influence on the presence and nature of their dynamics. Initial analysis of Li_6PS_5CN found that CN^- was distributed across the 4*a* and 4*d* Wyckoff positions and was orientationally disordered.[107] This led to the hypothesis that CN^- may undergo dynamic rotations that allow for a lowered activation energy for Li^+ hopping relative to Li_6PS_5Br.[107] Further molecular dynamics investigations revealed that the rotational dynamics of CN^- anions are highly dependent on S^{2-}/CN^- site mixing, with greater degrees of site mixing corresponding to slower and more constrained rotational dynamics, such as "wobbling in a cone" motions (Figure 16).[108] This phenomenon is hypothesized to be driven by CN^--CN^- elastic dipole coupling. In ordered configurations with no S^{2-}/CN^- disorder, each CN^- is ∼7 Å from its nearest CN^- neighbor.[108] However, in configurations with S^{2-}/CN^- site mixing, the CN^--CN^- distances are reduced, which increases elastic dipole coupling and increases the energetic cost for rotations.[108]

The apparent tunability of CN^- dynamics based on site disorder may provide an opportunity to investigate the influence of rotationally active pseudohalides upon PS_4^{3-} dynamics. The time scales and nature of CN^- rotations can be tuned via manipulating S^{2-}/CN^- site disorder, which can be modulated via alloying with a halide or through varying the S^{2-}/CN^- ratio.[108,138] The potential to activate or deactivate CN^- rotational dynamics may allow for a systematic study of how CN^- rotational disorder influences PS_4^{3-} dynamics. In $Li_6PS_5BH_4$, even the nature of BH_4^- rotational behavior remains unclear. Some open questions in this area include:

https://doi.org/10.1021/acs.chemmater.5c02939
Chem. Mater. 2026, 38, 3038−3058

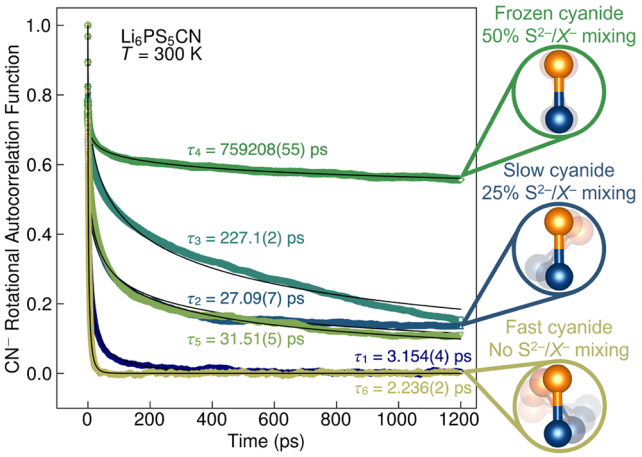

Figure 16. Rotational autocorrelation function for cyanide ions calculated for different configurations of anion site disorder. MD simulations were performed at $T = 300$ K. For fully ordered Li_6PS_5CN, rapid tumbling is observed on the picosecond time scale (τ_1, τ_6). Introduction of 25% anion disorder slows rotational dynamics by an order of magnitude (τ_2, τ_5) and inhibits full rotations, presumably favoring oscillatory or wobbling behaviors. At 50% anion site mixing, rotational dynamics occur on timescales ranging from hundreds to hundreds of thousands of picoseconds, indicating that rotational dynamics are significantly slowed and constrained to libratory behavior. Adapted from ref 108. Copyright 2024 American Chemical Society.

- How do the presence and timescales of pseudohalide dynamics impact rotational motions of larger tetrahedral units, and vice versa?
- To what extent do pseudohalide rotations couple to neighboring thiophosphate units, lithium ions, or both?
- Do uncoupled rotations lead to an enhancement of the dynamic bottleneck areas and vibrational environment modifications discussed in Section 6.1?

6.3. Coupled Dynamics

The proclivity for argyrodites to exhibit rotational disorder of polyhedral and molecular species (Sections 6.1 and 6.2) motivates the possibility for *coupled dynamics* between rotationally active species and ion migration. Polyhedral and molecular rotations have long been thought to facilitate ion transport; the extent of coupling and underlying mechanisms vary across material families and has been the subject of controversy since the 1980s.[47,171,174−181] The "paddlewheel" mechanism is characterized by large-amplitude rotations of the polyhedral species that are proposed to *actively* couple to Li^+ hopping (Figure 17a).[47,179] In contrast, a responsive "soft cradle" mechanism has been proposed, in which polyhedral or molecular units reorient to accommodate ion motion (Figure 17b).[178] A third proposed mechanism involves a gate or percolation model where vibrations and rotations of polyanions are not coupled with cation hopping, but transiently open low-energy conduction pathways through which ions can transit.[47,167,168,182,182] Although the precise mechanisms remain controversial, there is consensus that the dynamics of polyhedral or molecular reorientations are generally beneficial for ion transport.[47,180,181]

The relative timescales of rotational dynamics and mobile ion hopping provide insight into the potential for coupled dynamics.[49,178,179,183] As discussed above, the argyrodites may exhibit dynamics of both polyhedral and molecular species; the timescales of these motions are sensitive to the local environment. PS_4^{3-} rotations in Li_6PS_5Cl occur at a rate of approximately 10^9 s^{-1} at $T = 283$ K, while Li_6PS_5Br and Li_6PS_5I reach this rate at $T = 233$ K and $T = 223$ K, respectively.[49] Molecular dynamics (MD) simulations indicate that Li^+ hop *transit times* (τ_{hop})—the time from the beginning to end of an individual successful hop—are on the order of 10^{-12} s.[22,149] Thus, polyhedral rotational dynamics occur roughly 3 orders of magnitude more slowly than *individual* Li^+ hops, indicating that polyhedral dynamics are temporally decoupled from individual Li^+ hops. Similarly, lithium and cyanide dynamics occur on distinct timescales in the cyanide argyrodite Li_6PS_5CN; according to MD simulations, anion-ordered structures enable faster cyanide rotational dynamics ($\sim 10^{-12}$ s) and yield slower Li^+ dynamics ($\sim 10^{-9}$ s), while anion-disorder results in fast Li^+ hopping ($\sim 10^{-11}$ s) but slow or frozen cyanide rotations ($<10^{-7}$ s).[108]

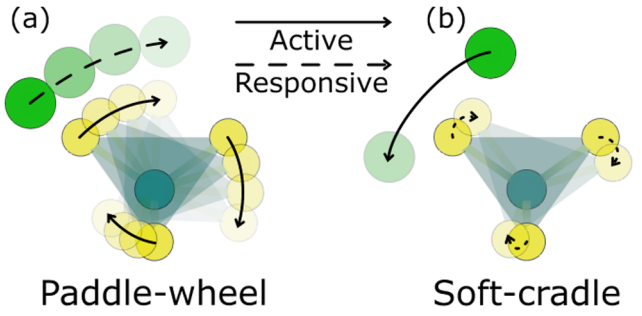

Figure 17. Illustration of two proposed mechanisms by which PS_4^{3-} rotations can couple directly to Li^+ dynamics. In the paddle-wheel mechanism (a), active rotations of PS_4^{3-} facilitate responsive Li^+ transport. In the soft-cradle mechanism (b), PS_4^{3-} rotates in response to Li^+ hops.

In the case of Li_6PS_5Cl and Li_6PS_5Br, PS_4^{3-} rotation rates ($1/\tau_{rot}$) approach the rate of *successful* Li^+ hopping ($1/\tau_{suc}$; $\approx 10^9$ s^{-1}), which may indicate Li^+-PS_4^{3-} coupling (Figure 12).[49,125,131] It is important to note that $\tau_{suc} \neq \tau_{hop}$; $1/\tau_{suc}$ corresponds to the rate at which successful hopping events occur, while τ_{hop} is the amount of time it takes for a single successful hop to occur from beginning to end. The similar values of $1/\tau_{rot}$ and $1/\tau_{suc}$ indicate that Li^+ jump attempts are successful on the same time scale that PS_4^{3-} units rotate and PS_4^{3-} units may be *causally implicated* in those jumps. The much faster time scale of τ_{hop} than τ_{rot} indicates that individual hops are completed far more quickly than polyhedral rotations, implying that the two processes are *temporally decoupled*.

Computational investigations of the argyrodites indicate that MCh_4 dynamics strongly influence ion transport. A recent study on Li_6PS_5Cl indicated that freezing PS_4^{3-} units in place was deleterious to ion transport, but that allowing them to translate and rotate effectively recovered ion diffusion properties.[149] Further, simulations in which PS_4^{3-} units are allowed to rotate about their central phosphorus indicate that these rotations nearly double Li^+ diffusivity in Li_6PS_5Cl relative to the static PS_4^{3-} control.[184] However, PSe_4^{3-} translational rather than rotational dynamics appear to be the main factor correlated with Cu^+ mobility in aristotypic Cu_7PSe_6.[97] Although PSe_4^{3-} rotations were not considered crucial in Cu^+ transport, no simulations in which PSe_4^{3-} rotations were allowed without translational freedom were performed.[97] Cooperative translational-rotational

https://doi.org/10.1021/acs.chemmater.5c02939
Chem. Mater. 2026, 38, 3038−3058

motions may serve to dynamically modulate ion transport bottlenecks or actively shuttle ions through the lattice.

The timescales and amplitudes of polyhedral rotations in Li_6PS_5X suggest a combination of gate-like modification of ion transport pathways and soft-cradle accommodation of Li^+. Systems in which polyhedral rotations significantly exceed the upper bound for librations (~30°) are often considered candidates for paddlewheel dynamics, although some studies define full 120° C_3 tetrahedral rotations as necessary in PS_4^{3-}-containing systems.[178,179] From local structure studies of Li_6PS_5X, the PS_4^{3-} tetrahedra exhibit relatively low-amplitude librations with rotation angles < 25° (Figure 14d) that are insufficient for a paddlewheel mechanism.[178] Rather, we propose that the relatively low-angle polyhedral rotations where the rotation rate is slower than or on the same order as ion hopping processes give rise to widened ion transport pathways that persist long enough for mobile ions to traverse the relevant bottlenecks (Figure 15a and b). This mechanism is reminiscent of the proposed "gate action" in Li_2SO_4, where SO_4^{2-} opens and closes ion conduction pathways as it undergoes rotations.[47,182] This gate-type mechanism most likely operates in tandem with a soft-cradle effect; the equilibrium orientations about which PS_4^{3-} units oscillate shift to accommodate local cation arrangements, consistent with computational studies that suggest translational and rotational dynamics contribute to transport.[97,149,184] This proposed mechanism can be considered pseudostatic—so long as the lifetime of the widened bottleneck (τ_{open}) exceeds the time required for an ion to traverse it (τ_{hop}), the effective bottleneck area governing transport is the maximum area sampled as the polyhedral units librate. In this limit ($\tau_{open} \gg \tau_{hop}$), transient structural distortions contribute to transport in much the same way as static bottleneck expansion. This pseudostatic picture is supported by the observation that polyhedral rotational dynamics occur roughly 3 orders of magnitude more slowly than individual Li^+ hops.[49,149]

Although NMR relaxometry highlights differences in rotation *rates* across Li_6PS_5X compositions, our pseudostatic view implies that *amplitude*, rather than frequency, is the transport-relevant variable. Our recent work demonstrated that PS_4^{3-} rotational displacements increased across the $Li_6PS_5I \rightarrow Li_6PS_5Br \rightarrow Li_6PS_5Cl$ series.[38] Taken together, these results suggest that the tetrahedra in Li_6PS_5I undergo rapid but shallow oscillations, producing small bottleneck fluctuations, while those in Li_6PS_5Cl undergo slower and larger oscillations that more substantially widen ion-transport pathways, with intermediate behavior in Li_6PS_5Br. Because $\tau_{open} \gg \tau_{hop}$, differences in rotation rates are unlikely to disrupt the pseudostatic picture. Rather, the larger rotational amplitudes in Li_6PS_5Br and Li_6PS_5Cl are sufficient to lower E_A, while the fast but shallow rotations in Li_6PS_5I inhibit transport and yield higher E_A values. The proposed "gate" mechanism is also consistent with the well-established design principle that anion antisite disorder lowers the energetic barriers for intercage hopping. Anion site disorder is associated with larger-amplitude tetrahedral rotations that widen the bottlenecks for ion hopping. Coupled with the electrostatic averaging picture described in Section 4, this observation may explain why relatively small degrees of anion site disorder (<10%) can have large impacts on macroscopic ionic conductivity.[161]

Given the shared structural and dynamic features between argyrodites and other materials systems comprised of dynamic polyhedral species, further investigation of libration-assisted transport and associated phase behavior is warranted. Several open questions that may clarify the underlying mechanisms are outlined below:

- Do polyanion librations occur independently of cation hopping—merely opening enthalpically and entropically favorable diffusion pathways—or do cation hops actively induce responsive polyanion rotations?
- By what mechanism does the incorporation of lower-valent anions stabilize high-temperature, fast-ion-conducting phases?
- Are polyanion libration amplitudes significantly altered in low-temperature phases compared to room-temperature-stabilized high-temperature phases?

7. CONCLUSIONS AND OUTLOOK

This Perspective seeks to establish the structure-dynamics-property relationships that underpin the exceptional ion transport properties of the argyrodite family.

7.1. Interplay of Site Disorder and Dynamics

Anion site disorder remains a common, underlying design principle for ion transport in the argyrodites. In the context of this Perspective, site disorder appears to be strongly coupled to the complex dynamics in the argyrodite structure. The same electrostatic averaging across the 4*a* and 4*d* sites that gives rise to long-range Li^+ percolation networks facilitates larger-amplitude polyanion rotations that take on a gate-like function to lower energetic barriers for intercage hopping. Concurrently, the onset of site disorder is associated with a noncompensatory drop in E_A and increase in σ_0, contrary to Meyer-Neldel behavior. Further, σ_0 scales exponentially with both site disorder and polyhedral displacement, implying that ΔS_m is modulated by the two factors. We hypothesize that site disorder promotes large amplitude oscillations of polyhedral units, which generate a broader distribution of vibrational environments and increase ΔS_m. This points to an emerging relationship between site disorder, polyhedral rotations, and ion transport.

7.2. Phase Transitions

The aristotype-hettotype relationship is core to understanding the behavior of argyrodites. The adoption of an aristotypic $F\bar{4}3m$ average structure with ordered MCh_4 tetrahedral units and delocalized mobile cation density is central to the argyrodite family. Low temperature hettotypes of the family represent minor modulations of the aristotype, generally with (a) localization of cations, (b) minor displacement of "free" anions, and (c) rotational modulations of the MCh_4 tetrahedra. The hettotype-aristotype transition is best described as an order–disorder phase transition, where activation of polyhedral rotations leads to dynamic sampling of local hettotype arrangements that average to the high-symmetry aristotype at sufficiently long length scales. This behavior is captured by Bragg diffraction that can be well fit by the $F\bar{4}3m$ aristotype and local structure that is best described by hettotype structures or an $F\bar{4}3m$ structure with rotationally modulated polyhedra. This phase behavior is shared by the Na_3PS_4 family of fast ion conductors and can be stabilized by the incorporation of lower-valent anions; halide substitution in the argyrodites commonly stabilizes the aristotype at room temperature. We propose that this effect is due to halide substitution lowering the energy required to activate polyhedral rotational dynamics by

https://doi.org/10.1021/acs.chemmater.5c02939
Chem. Mater. 2026, 38, 3038−3058

weakening the electrostatic interactions between MCh_4 units and "free" anion sites.

7.3. Future Directions

The richness of the dynamics and the interplay of static and dynamic disorder in these materials motivate several future directions for study.

- *Electrostatic Averaging vs Polyhedral Rotations:* At this stage, it is unclear whether electrostatic averaging due to site disorder is solely responsible for improved ion transport in argyrodites, or if activation of polyhedral dynamics through site disorder synergistically enhances ion transport. The causal relationships between site disorder, polyhedral dynamics, and improved ion transport should be interrogated to determine how polyhedral dynamics mediate between the other two.
- *Dynamic Disorder as a Defining Characteristic:* Our analysis of the argyrodite family predicts that dynamic disorder is inherent to the aristotype and therefore *all* aristotypic argyrodites will exhibit non-$F\bar{4}3m$ local symmetry. This behavior has been demonstrated in Li_6PS_5X and a selection of Ag^+-argyrodites, but further investigation to probe whether it is generalizable would be of great use to the field.
- *Aristotype Stabilization:* We hypothesize that halide substitution in the argyrodites stabilizes the aristotype by weakening electrostatic interactions between MCh_4 units and "free" anions, thereby lowering the energy required for polyhedral rotations. This, in turn, is proposed to contribute to the observed phase transition behavior. Testing this hypothesis would provide insight as to how fast ion conducting phases may be stabilized at room temperature.

Argyrodites are compositionally diverse, structurally complex, and exhibit rich dynamic phenomena that are important for ion transport. A deeper, quantitative understanding of lattice dynamics, local polyanion rotations, and their coupling with mobile ions will not only clarify transport mechanisms in argyrodites but also inform broader design strategies for dynamic, fast-ion-conducting solids.

AUTHOR INFORMATION

Corresponding Author

Annalise E. Maughan − *Department of Chemistry, Colorado School of Mines, Golden, Colorado 80401, United States; National Laboratory of the Rockies, Golden, Colorado 80401, United States;* orcid.org/0000-0002-3292-4799; Email: amaughan@mines.edu

Authors

Austin M. Shotwell − *Department of Chemistry, Colorado School of Mines, Golden, Colorado 80401, United States;* orcid.org/0000-0002-1264-8934

Shelby L. Galinat − *Materials Science Program, Colorado School of Mines, Golden, Colorado 80401, United States;* orcid.org/0000-0002-8520-0997

Complete contact information is available at: https://pubs.acs.org/10.1021/acs.chemmater.5c02939

Notes

The authors declare no competing financial interest.

Biographies

Austin M. Shotwell is a Ph.D. candidate in the research group of Dr. Annalise Maughan at the Colorado School of Mines. He received his B.S. in Chemistry and Politics from Centre College in 2021. His research investigates how local and long-range structures govern ion transport in solid electrolytes, particularly when the two length scales appear to disagree.

Shelby L. Galinat received her B.S. in Chemistry from the University of Utah in Salt Lake City. She is a National Science Foundation Graduate Research Fellow in the group of Dr. Annalise Maughan at the Colorado School of Mines who specializes in solution-phase synthesis of sulfide ion conductors. She is especially interested in dipole substitution and complex dynamics in argyrodites.

Dr. Annalise E. Maughan is an Assistant Professor in the Department of Chemistry at the Colorado School of Mines and holds a joint appointment with the National Laboratory of the Rockies. Her research program is focused on solid-state materials chemistry for energy, with an emphasis on understanding the fundamental principles that connect chemistry, local and long-range structure, and dynamics to functional properties such as charge transport and light absorption/emission.

ACKNOWLEDGMENTS

The authors thank Tyler Case and Prof. David Halat for insightful discussions. This work was supported by the U.S. Department of Energy's Transportation Technologies Office (TTO) under the Low-Pressure All-Solid-State Cells project, directed by Simon Thompson and Tien Duong and managed by Anthony Burrell. S.L.G. acknowledges support from the National Science Foundation Graduate Research Fellowship Program under Grant No. DGE-2137099. S.L.G. and A.E.M. acknowledge support from the National Science Foundation under Award No. DMR-2339634. A.M.S. and S.L.G. acknowledge Johann Wolfgang von Goethe's "Der Fischer" for providing constant inspiration and enlightenment in parsing the complex interplay of dynamic polyhedra and mobile ions. This work was authored in part by the National Laboratory of the Rockies for the U.S. Department of Energy (DOE), operated under Contract No. DE-AC36-08GO28308. Funding provided by the U.S. Department of Energy Critical Minerals and Energy Innovation Vehicle Technologies Office. The views expressed in the article do not necessarily represent the views of the DOE or the U.S. Government.

REFERENCES

(1) Winkler, C. Germanium Ge, ein neues, nichtmetallisches Element. *Ber. Dtsch. Chem. Ges.* **1886**, *19*, 210−211.

(2) Bletskan, D.; Vakulchak, V.; Studenyak, I. Ab Initio Calculations of the Band Structure and Optical Properties of Ag_7SiS_5I. *AIP Conf Proc.* **2020**, *2220*, 100010.

(3) Pogodin, A. I.; Pop, M. M.; Shender, I. A.; Filep, M. J.; Malakhovska, T. O.; Vakulchak, V. V.; Kokhan, O. P.; Bletskan, D.; Rubish, V. M.; Lisý, V.; et al. Band Structure and Optical Properties of Low Temperature Modification of Ag_7PS_6 Single Crystal. *J. Mater. Sci.: Mater. Electron.* **2023**, *34*, 1508.

(4) Kranjčec, M.; Studenyak, I. P.; Kovács, G. S.; Mitrovcij, V. V. Compositional Disordering and Some Structural and Optical Parameters of $Cu_6P(S_{1-x}Se_x)_5Br$ Mixed Crystals. *Mater. Sci. Eng., B* **2002**, *95*, 107−110.

(5) Ibrar, M.; Murtaza, G.; Haneef, M.; Jehangir, M. A.; Alotaibi, N. H.; Mohammad, S.; Bashir, B.; Zaman, T. Elastic-acoustic, Optical and Thermoelectric Investigation of Cu_6AsS_5X (X= Br,I) for Renewable Energy Applications. *Comput. Condens. Matter.* **2024**, *40*, No. e00946.

(6) Kranjčec, M.; Studenyak, I. P.; Kovacs, G. S.; Desnica Franković, I. D.; Panko, V. V.; Guranich, P. P.; Slivka, V. Y. Electric Conductivity and Optical Absorption Edge of $Cu_6P(Se_xS_{1-x})_5$ I Fast-Ion Conductors in the Selenium-Rich Region. *J. Phys. Chem. Solids* **2001**, *62*, 665−672.
(7) Studenyak, I. P.; Kranjčec, M.; Kovács, G. S.; Desnica-Franković, I. D.; Molnar, A. A.; Panko, V. V.; Slivka, V. Y. Electrical and Optical Absorption Studies of Cu_7GeS_5I Fast-ion Conductor. *J. Phys. Chem. Solids* **2002**, *63*, 267−271.
(8) Studenyak, I.; Kayla, M.; Kranjčec, M.; Kokhan, O.; Minets, Y. Isoabsorption and Spectrometric Studies of Optical Absorption Edge in Cu_6AsS_5I Superionic Crystal. *J. Phys. Chem. Solids* **2011**, *72*, 1419−1422.
(9) Gao, L.; Wu, X.; Yang, D.; Tian, X.; Xu, J.; Zhang, B.; Wu, K. M_6PS_5X (M = Ag, Cu; X = Cl, Br) Chalcohalides Exhibiting Strong Nonlinear Optical Responses and High Laser Damage Resistances. *Dalton Trans.* **2021**, *50*, 17901−17905.
(10) Wang, B.; Li, S.; Luo, Y.; Yang, J.; Ye, H.; Liu, Y.; Jiang, Q. A New Thermoelectric Ag_8SiSe_6 Argyrodite for Room Temperature Application: Sensitivity of Thermoelectric Performance to Cooling Conditions. *Mater. Adv.* **2024**, *5*, 3735−3741.
(11) Jiang, Q.; Li, S.; Luo, Y.; Xin, J.; Li, S.; Li, W.; Zhao, G.; Yang, J. Ecofriendly Highly Robust Ag_8SiSe_6-Based Thermoelectric Composites with Excellent Performance Near Room Temperature. *ACS Appl. Mater. Interfaces* **2020**, *12*, 54653−54661.
(12) Andriyevsky, B.; Barchiy, I. E.; Studenyak, I. P.; Kashuba, A. I.; Piasecki, M. Electron Phonon and Thermoelectric Properties of Cu_7PS_6 Crystal Calculated at DFT Level. *Sci. Rep.* **2021**, *11*, 19065.
(13) Fan, Y.; Wang, G.; Wang, R.; Zhang, B.; Shen, X.; Jiang, P.; Zhang, X.; Gu, H.-S.; Lu, X.; Zhou, X.-Y. Enhanced Thermoelectric Properties of P-type Argyrodites Cu_8GeS_6 Through Cu Vacancy. *J. Alloys Compd.* **2020**, *822*, 153665.
(14) Heep, B. K.; Weldert, K. S.; Krysiak, Y.; Day, T. W.; Zeier, W. G.; Kolb, U.; Snyder, G. J.; Tremel, W. High Electron Mobility and Disorder Induced by Silver Ion Migration Lead to Good Thermoelectric Performance in the Argyrodite Ag_8 $SiSe_6$. *Chem. Mater.* **2017**, *29*, 4833−4839.
(15) Shen, X.; Yang, C.-C.; Liu, Y.; Wang, G.; Tan, H.; Tung, Y.-H.; Wang, G.; Lu, X.; He, J.; Zhou, X. High-Temperature Structural and Thermoelectric Study of Argyrodite Ag_8GeSe_6. *ACS Appl. Mater. Interfaces* **2019**, *11*, 2168−2176.
(16) Zaman, T.; Ullah, M.; Chaudhry, A. R.; Ibrar, M.; Jehangir, M. A.; Saeed, M.; Haneef, M.; Murtaza, G. Optoelectronic, Thermoelectric, and Elastic Properties of Cu_6PSe_5X (X = Br, I) Argyrodites Using Density Functional Theory. *Phys. Scr.* **2024**, *99*, 1159106.
(17) Zong, P.-A.; Li, Y.; Negishi, R.; Li, Z.; Zhang, C.; Wan, C. Thermoelectric Performance of Cu_8SiS_6 with High Electronic Band Degeneracy. *ACS Appl. Electron. Mater.* **2024**, *6*, 2832−2838.
(18) Kraft, M. A.; Culver, S. P.; Calderon, M.; Böcher, F.; Krauskopf, T.; Senyshyn, A.; Dietrich, C.; Zevalkink, A.; Janek, J.; Zeier, W. G. Influence of Lattice Polarizability on the Ionic Conductivity in the Lithium Superionic Argyrodites Li_6PS_5X (X = Cl, Br, I). *J. Am. Chem. Soc.* **2017**, *139*, 10909−10918.
(19) Minafra, N.; Kraft, M. A.; Bernges, T.; Li, C.; Schlem, R.; Morgan, B. J.; Zeier, W. G. Local Charge Inhomogeneity and Lithium Distribution in the Superionic Argyrodites Li_6PS_5X (X = Cl, Br, I). *Inorg. Chem.* **2020**, *59*, 11009−11019.
(20) Ohno, S.; Helm, B.; Fuchs, T.; Dewald, G.; Kraft, M. A.; Culver, S. P.; Senyshyn, A.; Zeier, W. G. Further Evidence for Energy Landscape Flattening in the Superionic Argyrodites $Li_{6+x}P_{1-x}M_xS_5I$ (M = Si, Ge, Sn). *Chem. Mater.* **2019**, *31*, 4936−4944.
(21) de Klerk, N. J. J.; Rosłoń, I.; Wagemaker, M. Diffusion Mechanism of Li Argyrodite Solid Electrolytes for Li-Ion Batteries and Prediction of Optimized Halogen Doping: The Effect of Li Vacancies, Halogens, and Halogen Disorder. *Chem. Mater.* **2016**, *28*, 7955−7963.
(22) Morgan, B. J. Mechanistic Origin of Superionic Lithium Diffusion in Anion-Disordered Li_6PS_5X Argyrodites. *Chem. Mater.* **2021**, *33*, 2004−2018.
(23) Sadowski, M.; Albe, K. Influence of Br^-/S^{2-} site — Exchange on Li Diffusion Mechanism in Li_6PS_5Br — a Computational Study. *Philos Trans A Math Phys Eng Sci* **2021**, *379*, 20190458.
(24) Hogrefe, K.; Minafra, N.; Hanghofer, I.; Banik, A.; Zeier, W. G.; Wilkening, H. M. R. Opening Diffusion Pathways through Site Disorder: The Interplay of Local Structure and Ion Dynamics in the Solid Electrolyte $Li_{6+x}P_{1-x}Ge_xS_5I$ as Probed by Neutron Diffraction and NMR. *J. Am. Chem. Soc.* **2022**, *144*, 1795−1812.
(25) Zhou, L.; Zhang, Q.; Nazar, L. F. Li-Rich and Halide-Deficient Argyrodite Fast Ion Conductors. *Chem. Mater.* **2022**, *34*, 9634−9643.
(26) Wei, P.-C.; Hsing, C.-R.; Yang, C.-C.; Tung, Y.-H.; Wu, H.-J.; Yen, W.-T.; Lai, Y.-C.; Lee, J.-J.; Wang, C.-W.; Wu, H.-C.; et al. Liquid-Like Thermal Conductivity in Solid Materials: Dynamic Behavior of Silver Ions in Argyrodites. *Nano Energy* **2024**, *122*, 109324.
(27) Al-Kutubi, H.; Gautam, A.; Lavrinenko, A. K.; Vasileiadis, A.; Heringa, J. R.; Ganapathy, S.; Wagemaker, M. Decoding Structural Disorder, Synthesis Methods, and Short- and Long-Range Lithium-Ion Transport in Lithium Argyrodites ($Li_{6-x}PS_{5-x}Br_{1+x}$). *Chem. Mater.* **2025**, *37*, 869−883.
(28) Zhou, R.; Gautam, A.; Suard, E.; Li, S.; Ganapathy, S.; Chen, K.; Zhang, X.; Nan, C.-W.; Wang, S.; Wagemaker, M. Boosting Ionic Conductivity and Air Stability in Bromide-Rich Thioarsenate Argyrodite Solid Electrolytes. *Adv. Funct. Mater.* **2025**, *35*, 2420971.
(29) Ren, Q.; Gupta, M. K.; Jin, M.; Ding, J.; Wu, J.; Chen, Z.; Lin, S.; Fabelo, O.; Rodríguez-Velamazán, J. A.; Kofu, M.; et al. Extreme Phonon Anharmonicity Underpins Superionic Diffusion and Ultralow Thermal Conductivity in Argyrodite Ag_8SnSe_6. *Nat. Mater.* **2023**, *22*, 999−1006.
(30) Zhang, Z.; Yu, C.; Xu, R.; Peng, L.; Ren, H.; Zhang, J.; Zhang, L.; Cheng, S.; Xie, J. Iodine-Rich Lithium Argyrodite with Enhanced Ionic Conductivity for Solid-state Batteries. *Scr. Mater.* **2022**, *210*, 114475.
(31) Belin, R.; Zerouale, A.; Pradel, A.; Ribes, M. Ion Dynamics in the Argyrodite Compound Ag_7GeSe_5I: Non-Arrhenius Behavior and Complete Conductivity Spectra. *Solid State Ion.* **2001**, *143*, 445−455.
(32) Deiseroth, H.-J.; Maier, J.; Weichert, K.; Nickel, V.; Kong, S.-T.; Reiner, C. Li_7PS_6 and Li_6PS_5X (X: Cl, Br, I): Possible Three-Dimensional Diffusion Pathways for Lithium Ions and Temperature Dependence of the Ionic Conductivity by Impedance Measurements. *Z. Anorg. Allg. Chem.* **2011**, *637*, 1287−1294.
(33) Kuhs, W. F.; Nitsche, R.; Scheunemann, K. The Argyrodites — a New Family of Tetrahedrally Close-Packed Structures. *Mater. Res. Bull.* **1979**, *14*, 241−248.
(34) Zhou, L.; Assoud, A.; Zhang, Q.; Wu, X.; Nazar, L. F. New Family of Argyrodite Thioantimonate Lithium Superionic Conductors. *J. Am. Chem. Soc.* **2019**, *141*, 19002−19013.
(35) Wang, Y.; Bazak, J. D.; Zhou, L.; Zhang, Q.; Singh, B.; Nazar, L. F. Liquid-Like Solid-State Diffusion of Lithium Ions in Super-Halide-Rich Argyrodite. *Cell Rep. Phys. Sci.* **2024**, *5*, 102314.
(36) Wang, P.; Patel, S.; Liu, H.; Chien, P.-H.; Feng, X.; Gao, L.; Chen, B.; Liu, J.; Hu, Y.-Y. Configurational and Dynamical Heterogeneity in Superionic $Li_{5.3}PS_{4.3}Cl_{1.7-x}Br_x$. *Adv. Funct. Mater.* **2023**, *33*, 2307954.
(37) Babanly, M. B. A.; Yusibov, Y.; Imamaliyeva, S. Z. M.; Babanly, D. J.; Alverdiyev, J. I. Alverdiyev, I. Phase Diagrams in the Development of the Argyrodite Family Compounds and Solid Solutions Based on Them. *J. Phase Equilib. Diffus.* **2024**, *45*, 228−255.
(38) Shotwell, A. M.; Schulze, M. C.; Yox, P.; Alaniz, C.; Maughan, A. E. Tetrahedral Tilting and Lithium-Ion Transport in Halide Argyrodites Prepared by Rapid, Microwave-Assisted Synthesis. *Adv. Funct. Mater.* **2025**, *35*, 2500237.
(39) Kang, T.; Li, C.; Zhang, X.; Nakamura, Y.; Tseng, J.-C.; Manjo, T.; Liu, C.; Yang, L. Local Symmetry Breaking Induced Superionic Conductivity in Argyrodites. *J. Am. Chem. Soc* **2026**, *148*, 6158−6166.
(40) Schlenker, R.; Hansen, A.-L.; Senyshyn, A.; Zinkevich, T.; Knapp, M.; Hupfer, T.; Ehrenberg, H.; Indris, S. Structure and Diffusion Pathways in Li_6PS_5Cl Argyrodite from Neutron Diffraction, Pair-Distribution Function Analysis, and NMR. *Chem. Mater.* **2020**, *32*, 8420−8430.
(41) Famprikis, T.; Bouyanfif, H.; Canepa, P.; Zbiri, M.; Dawson, J. A.; Suard, E.; Fauth, F.; Playford, H. Y.; Dambournet, D.; Borkiewicz, O. J.;

et al. Insights into the Rich Polymorphism of the Na^+ Ion Conductor Na_3PS_4 from the Perspective of Variable-Temperature Diffraction and Spectroscopy. *Chem. Mater.* **2021**, *33*, 5652−5667.
(42) Maus, O.; Agne, M. T.; Fuchs, T.; Till, P. S.; Wankmiller, B.; Gerdes, J. M.; Sharma, R.; Heere, M.; Jalarvo, N.; Yaffe, O.; et al. On the Discrepancy Between Local and Average Structure in the Fast Na^+ Ionic Conductor $Na_{2.9}Sb_{0.9}W_{0.1}S_4$. *J. Am. Chem. Soc.* **2023**, *145*, 7147−7158.
(43) Ghata, A.; Bernges, T.; Maus, O.; Wankmiller, B.; Naik, A. A.; Bustamante, J.; Gaultois, M. W.; Delaire, O.; Hansen, M. R.; George, J.; et al. Exploring the Thermal and Ionic Transport of Cu^+ Conducting Argyrodite Cu_7PSe_6. *Adv. Energy Mater.* **2024**, *14*, 2402039.
(44) Nagel, A.; Range, K.-J. Verbindungsbildung im System Ag_2S-GeS_2-AgI/Compound Formation in the System Ag_2S-GeS_2-AgI. *Z. Naturforsch. B* **1978**, *33*, 1461−1464.
(45) Beeken, R. B.; Garbe, J. J.; Petersen, N. R. Cation Mobility in the Cu_6PS_5X (X = Cl, Br, I) Argyrodites. *J. Phys. Chem. Solids* **2003**, *64*, 1261−1264.
(46) Kong, S.-T.; Deiseroth, H.-J.; Reiner, C.; Gün, Ö.; Neumann, E.; Ritter, C.; Zahn, D. Lithium Argyrodites with Phosphorus and Arsenic: Order and Disorder of Lithium Atoms, Crystal Chemistry, and Phase Transitions. *Chem. Eur. J.* **2010**, *16*, 2198−2206.
(47) Jansen, M. Volume Effect or Paddle-Wheel Mechanism—Fast Alkali-Metal Ionic Conduction in Solids with Rotationally Disordered Complex Anions. *Angew. Chem. Int. Ed.* **1991**, *30*, 1547−1558.
(48) Krauskopf, T.; Culver, S. P.; Zeier, W. G. Local Tetragonal Structure of the Cubic Superionic Conductor Na_3PS_4. *Inorg. Chem.* **2018**, *57*, 4739−4744.
(49) Hanghofer, I.; Gadermaier, B.; Wilkening, H. M. R. Fast Rotational Dynamics in Argyrodite-Type Li_6PS_5X (X: Cl, Br, I) as Seen by ^{31}P Nuclear Magnetic Relaxation - On Cation-Anion Coupled Transport in Thiophosphates. *Chem. Mater.* **2019**, *31*, 4591−4597.
(50) Gautam, A.; Ghidiu, M.; Hansen, A.-L.; Ohno, S.; Zeier, W. G. Sn Substitution in the Lithium Superionic Argyrodite Li_6PCh_5I (Ch = S and Se). *Inorg. Chem.* **2021**, *60*, 18975−18980.
(51) Minafra, N.; Culver, S. P.; Krauskopf, T.; Senyshyn, A.; Zeier, W. G. Effect of Si Substitution on the Structural and Transport Properties of Superionic Li-Argyrodites. *J. Mater. Chem. A* **2018**, *6*, 645−651.
(52) Liu, Y.; Peng, H.; Su, H.; Zhong, Y.; Wang, X.; Xia, X.; Gu, C.; Tu, J. Ultrafast Synthesis of I-Rich Lithium Argyrodite Glass−Ceramic Electrolyte with High Ionic Conductivity. *Adv. Mater.* **2022**, *34*, 2107346.
(53) Adeli, P.; Bazak, J. D.; Park, K. H.; Kochetkov, I.; Huq, A.; Goward, G. R.; Nazar, L. F. Boosting Solid-State Diffusivity and Conductivity in Lithium Superionic Argyrodites by Halide Substitution. *Angew. Chem., Int. Ed.* **2019**, *58*, 8681−8686.
(54) Gautam, A.; Al-Kutubi, H.; Famprikis, T.; Ganapathy, S.; Wagemaker, M. Exploring the Relationship Between Halide Substitution, Structural Disorder, and Lithium Distribution in Lithium Argyrodites ($Li_{6-x}PS_{5-x}Br_{1+x}$). *Chem. Mater.* **2023**, *35*, 8081−8091.
(55) Brandt, G.; Krämer, V. Phase Investigations in the Silver-Gallium-Sulphur System. *Mater. Res. Bull.* **1976**, *11*, 1381−1388.
(56) Lin, S.; Li, W.; Bu, Z.; Gao, B.; Li, J.; Pei, Y. Thermoelectric Properties of Ag_9GaS_6 with Ultralow Lattice Thermal Conductivity. *Mater. Today Phys.* **2018**, *6*, 60−67.
(57) Hellstrom, E. E.; Schoonman, J. Silver Ionic and Electronic Conductivity in Ag_9GaS_6. *Solid State Ion.* **1980**, *1*, 199−210.
(58) Hellstrom, E. E.; Huggins, R. A. Silver Ionic and Electronic Conductivity in Ag_9GaS_6, Ag_9AlS_6, $AgGaS_2$, $AgAlS_2$, and $AgAl_5S_8$. *J. Solid State Chem.* **1980**, *35*, 207−214.
(59) Mikkelsen, J. C. Ag_2Se-Ga_2Se_3 Pseudobinary Phase Diagram. *Mater. Res. Bull.* **1977**, *12*, 497−502.
(60) Boivin, J.; Thomas, D.; Tridot, G. Contribution a Letude des Systemes-Sulfure de Silicium et Sulfur de Cuivre ou Dargent. *C. R. Hebd. Séances Acad. Sci., Sér. C* **1967**, *264*, 1286.
(61) Gorochov, O.; Flahaut, J. Les Composes Ag_8MX_6 Avec M= Si Ge Ss Et X= S Se Te. *C. R. Hebd. Séances Acad. Sci., Sér. C* **1967**, *264*, 2153.
(62) Bletskan, D.; Vakulchak, V.; Lisý, V.; Studenyak, I. Influence of Cationic Substitution on the Electronic Structure of Cu_7SiS_5I and Ag_7SiS_5I Compounds. *AIP Conf. Proc.* **2021**, *2369*, 020154.
(63) Boucher, F.; Evain, M.; Brec, R. Single-Crystal Structure Determination of λ-Ag_8SiTe_6 and Powder X-ray Study of Low-Temperature α and β phases. *J. Solid State Chem.* **1992**, *100*, 341−355.
(64) Munsif, M.; Shah, M. First Principles study of Silver Argyrodites-Structured Compounds A_8BC_6(A = Ag; B = Si, Ge; C = Te) for Opto-Electronic Application. *J. Environ. Chem.* **2023**, 40−51.
(65) Eulenberger, G. Die Kristallstruktur der Tieftemperaturmodifikation von Ag_8GeS_6. *Monatsh. Chem.* **1977**, *108*, 901−913.
(66) Pogodin, A. I.; Filep, M. J.; Izai, V. Y.; Kokhan, O. P.; Kus, P. Crystal Growth and Electrical Conductivity of Ag_7PS_6 and Ag_8GeS_6 Argyrodites. *J. Phys. Chem. Solids* **2022**, *168*, 110828.
(67) Studenyak, I.; Pogodin, A.; Shender, I.; Filep, M.; Kokhan, O.; Kopčanský, P. Electrical Properties of Cation-Substituted $Ag_7(Si_{1-x}Ge_x)S_5I$ Single Crystals. *Semicond. Phys., Quantum Electron. Optoelectron* **2021**, *24*, 241−247.
(68) Alverdiev, I. J.; Bagheri, S. M.; Aliyeva, Z. M.; Yusibov, Y. A.; Babanly, M. B. Phase Equilibria in the Ag_2Se-$GeSe_2$−$SnSe_2$ System and Thermodynamic Properties of $Ag_8Ge_{1-x}Sn_xSe_6$ Solid Solutions. *Inorg. Mater.* **2017**, *53*, 786−796.
(69) Albert, S.; Haines, J.; Granier, D.; Pradel, A.; Ribes, M. Effect of Pressure on the Superionic Argyrodite Ag_7GeSe_5I. *J. Appl. Crystallogr.* **2009**, *42*, 93−100.
(70) Albert, S.; Pillet, S.; Lecomte, C.; Pradel, A.; Ribes, M. Disorder in Ag_7GeSe_5I, a Superionic Conductor: Temperature-Dependent Anharmonic Structural Study. *Acta Crystallogr., Sect. B: Struct. Sci.* **2008**, *64*, 1−11.
(71) Boucher, F.; Evain, M.; Brec, R. Distribution and Ionic Diffusion Path of Silver in λ-Ag_8GeTe_6: A Temperature Dependent Anharmonic Single Crystal Structure Study. *J. Solid State Chem.* **1993**, *107*, 332−346.
(72) Slade, T. J.; Gvozdetskyi, V.; Wilde, J. M.; Kreyssig, A.; Gati, E.; Wang, L.-L.; Mudryk, Y.; Ribeiro, R. A.; Pecharsky, V. K.; Zaikina, J. V.; et al. A Low-Temperature Structural Transition in Canfieldite, Ag_8SnS_6, Single Crystals. *Inorg. Chem.* **2021**, *60*, 19345−19355.
(73) Piskach, L. V.; Parasyuk, O. V.; Olekseyuk, I. D.; Romanyuk, Y. E.; Volkov, S. V.; Pekhnyo, V. I. Interaction of Argyrodite Family Compounds with the Chalcogenides of II-b Elements. *J. Alloys Compd.* **2006**, *421*, 98−104.
(74) Hahn, H.; Schulze, H.; Sechser, L. Über einige ternäre Chalkogenide vom Argyrodit-Typ. *Naturwiss* **1965**, *52*, 451−451.
(75) Beeken, R. B.; Garbe, J. J.; Gillis, J. M.; Petersen, N. R.; Podoll, B. W.; Stoneman, M. R. Electrical Conductivities of the Ag_6PS_5X and the Cu_6PSe_5X (X = Br, I)Argyrodites. *J. Phys. Chem. Solids* **2005**, *66*, 882−886.
(76) Evain, M.; Gaudin, E.; Boucher, F.; Petricek, V.; Taulelle, F. Structures and Phase Transitions of the A_7PSe_6 (A = Ag, Cu) Argyrodite-Type Ionic Conductors. I. Ag_7PSe_6. *Acta Crystallogr., Sect. B: Struct. Sci.* **1998**, *54*, 376−383.
(77) Gaudin, E.; Boucher, F.; Evain, M.; Taulelle, F. NMR Selection of Space Groups in Structural Analysis of Ag_7PSe_6. *Chem. Mater.* **2000**, *12*, 1715−1720.
(78) Beeken, R. B.; Driessen, C. R.; Hinaus, B. M.; Pawlisch, D. E. Electrical Conductivity of Ag_7PSe_6 and Cu_7PSe_6. *Solid State Ion.* **2008**, *179*, 1058−1060.
(79) Beeken, R. B.; Garbe, J. J.; Petersen, N. R.; Stoneman, M. R. Electrical Properties of the Ag_6PSe_5X (X = Cl, Br, I) Argyrodites. *J. Phys. Chem. Solids* **2004**, *65*, 1011−1014.
(80) Carcaly, C.; Ollitrault-Fichet, R.; Houphouët, D.; Eholié, R.; Flahaut, J. Les Composes Ag_7AsS_6 et Ag_7AsSe_6 Etude des Proprietes Thermiques, Cristallographiques et Electriques. *Mater. Res. Bull.* **1979**, *14*, 1497−1503.
(81) Bindi, L.; Downs, R. T.; Menchetti, S. The Crystal Structure of Billingsleyite, $Ag_7(As,Sb)S_6$, a Sulfosalt Containing As^{5+}. *Can. Mineral* **2010**, *48*, 155−162.
(82) Thomas, D. Structural Analogy of Sulfurated Compounds Containing Barium or Silicon and Copper or Silver. *C. R. Hebd. Séances Acad. Sci., Sér. C* **1967**, *265*, 1325.
(83) Gao, L.; Lee, M.-H.; Zhang, J. Metal-Cation Substitutions Induced the Enhancement of Second Harmonic Generation in A_8BS_6

https://doi.org/10.1021/acs.chemmater.5c02939
Chem. Mater. 2026, 38, 3038−3058

(A = Cu, and Ag; B = Si, Ge, and Sn). *New J. Chem.* **2019**, *43*, 3719−3724.
(84) Ishii, M.; Onoda, M.; Chen, X.-A.; Wada, H.; Shibata, K. Vibrational Spectra and Phase Transitions of Cu_8MX_6 (M = Si, Ge; X = S, Se) and Cu_4GeS_4. *Solid State Ion.* **2000**, *136*−*137*, 403−407.
(85) Ishii, M.; Onoda, M.; Shibata, K. Structure and Vibrational Spectra of Argyrodite Family Compounds Cu_8SiX_6 (X = S, Se) and Cu_8GeS_6. *Solid State Ion.* **1999**, *121*, 11−18.
(86) Studenyak, I. P.; Kokhan, O. P.; Kranjčec, M.; Hrechyn, M. I.; Panko, V. V. Crystal Growth and Phase Interaction Studies in the Cu_7GeS_5I-Cu_7SiS_5I Superionic System. *J. Cryst. Growth* **2007**, *306*, 326−329.
(87) Bairamova, U. R.; Babanly, K. N.; Mashadieva, L. F.; Yusibov, Y. A.; Babanly, M. B. Phase Equilibria in the Cu_2Se-Cu_8SiSe_6-Cu_8GeSe_6 System. *Russ. J. Inorg. Chem.* **2023**, *68*, 1611−1621.
(88) Khanafer, M.; Gorochov, O.; Rivet, J. Etude des Proprietes Electriques des Phases: Cu_2GeS_3, Cu_2SnS_3, Cu_8GeS_6 et Cu_4SnS_4. *Mater. Res. Bull.* **1974**, *9*, 1543−1552.
(89) Alverdiyev, I. J.; Aliev, Z. S.; Bagheri, S. M.; Mashadiyeva, L. F.; Yusibov, Y. A.; Babanly, M. B. Study of the $2Cu_2S + GeSe_2$ $Cu_2Se + GeS_2$ Reciprocal System and Thermodynamic Properties of the $Cu_8GeS_{6-x}Se_x$ Solid Solutions. *J. Alloys Compd.* **2017**, *691*, 255−262.
(90) Onoda, M.; Chen, X.-A.; Kato, K.; Sato, A.; Wada, H. Structure Refinement of Cu_8GeS_6 Using X-ray Diffraction Data from a Multiple-Twinned Crystal. *Acta Crystallogr., Sect. B: Struct. Sci.* **1999**, *55*, 721−725.
(91) Onoda, M.; Ishii, M.; Pattison, P.; Shibata, K.; Yamamoto, A.; Chapuis, G. Superspace-Group Approach to the Phase Transition of Cu_8GeSe_6. *J. Solid State Chem.* **1999**, *146*, 355−362.
(92) Studenyak, I. P.; Kranjčec, M.; Bilanchuk, V. V.; Kokhan, O. P.; Orliukas, A. F.; Kezionis, A.; Kazakevicius, E.; Salkus, T. Temperature Variation of Electrical Conductivity and Absorption Edge in Cu_7GeSe_5I Advanced Superionic Conductor. *J. Phys. Chem. Solids* **2009**, *70*, 1478−1481.
(93) Shen, X.; Ouyang, N.; Huang, Y.; Tung, Y.-H.; Yang, C.-C.; Faizan, M.; Perez, N.; He, R.; Sotnikov, A.; Willa, K.; et al. Amorphous-Like Ultralow Thermal Transport in Crystalline Argyrodite Cu_7PS_6. *Adv. Sci.* **2024**, *11*, 2400258.
(94) Studenyak, I. P.; Kranjčec, M.; Kovács, G. S.; Pan'ko, V. V.; Desnica, I. D.; Slivka, A. G.; Guranich, P. P. The Effect of Temperature and Pressure on the Optical Absorption Edge in Cu_6PS_5X (X = Cl, Br, I) Crystals. *J. Phys. Chem. Solids* **1999**, *60*, 1897−1904.
(95) Gagor, A.; Pietraszko, A.; Kaynts, D. Structural Aspects of Fast Copper Mobility in Cu_6PS_5Cl — the Best Solid Electrolyte from Cu_6PS_5X Series. *J. Solid State Chem.* **2008**, *181*, 777−782.
(96) Kranjčec, M.; Studenyak, I. P.; Buchuk, R. Y.; Stephanovich, V. O.; Kökényesi, S.; Kis-Varga, M. Structural Properties and Raman Scattering in Cu_6PS_5X (X = I, Br)Nanocrystalline Solid Electrolytes. *Solid State Ion.* **2008**, *179*, 218−221.
(97) Gupta, M. K.; Ding, J.; Bansal, D.; Abernathy, D. L.; Ehlers, G.; Osti, N. C.; Zeier, W. G.; Delaire, O. Strongly Anharmonic Phonons and Their Role in Superionic Diffusion and Ultralow Thermal Conductivity of Cu_7PSe_6. *Adv. Energy Mater.* **2022**, *12*, 2200596.
(98) Nilges, T.; Pfitzner, A. A Structural Differentiation of Quaternary Copper Argyrodites: Structure — Property Relations of High Temperature Ion Conductors. *Z. Kristallogr Cryst. Mater.* **2005**, *220*, 281−294.
(99) Strauss, F.; Zinkevich, T.; Indris, S.; Brezesinski, T. Li_7GeS_5Br—An Argyrodite Li-Ion Conductor Prepared by Mechanochemical Synthesis. *Inorg. Chem.* **2020**, *59*, 12954−12959.
(100) Kong, S.-T.; Deiseroth, H.-J.; Maier, J.; Nickel, V.; Weichert, K.; Reiner, C. Li_6PO_5Br and Li_6PO_5Cl: the First Lithium-Oxide-Argyrodites. *Z. Anorg. Allg. Chem.* **2010**, *636*, 1920−1924.
(101) Kong, S. T.; Gün, Ö.; Koch, B.; Deiseroth, H. J.; Eckert, H.; Reiner, C. Structural Characterisation of the Li Argyrodites Li_7PS_6 and Li_7PSe_6 and Their Solid Solutions: Quantification of Site Preferences by MAS-NMR Spectroscopy. *Chem. Eur. J.* **2010**, *16*, 5138−5147.
(102) Kam, R. L.; Jun, K.; Barroso-Luque, L.; Yang, J. H.; Xie, F.; Ceder, G. Crystal Structures and Phase Stability of the Li_2S-P_2S_5 System from First Principles. *Chem. Mater.* **2023**, *35*, 9111−9126.
(103) Deiseroth, H.-J.; Kong, S.-T.-T.; Eckert, H.; Vannahme, J.; Reiner, C.; Zaiß, T.; Schlosser, M. Li_6PS_5X: A Class of Crystalline Li-Rich Solids with an Unusually High Li^+ Mobility. *Angew. Chem. Int.L Ed.* **2008**, *47*, 755−758.
(104) Stamminger, A. R.; Ziebarth, B.; Mrovec, M.; Hammerschmidt, T.; Drautz, R. Ionic Conductivity and Its Dependence on Structural Disorder in Halogenated Argyrodites Li_6PS_5X (X = Br, Cl, I). *Chem. Mater.* **2019**, *31*, 8673−8678.
(105) Sun, Y.; Ouyang, B.; Wang, Y.; Zhang, Y.; Sun, S.; Cai, Z.; Lacivita, V.; Guo, Y.; Ceder, G. Enhanced Ionic Conductivity and Lack of Paddle-Wheel Effect in Pseudohalogen-Substituted Li Argyrodites. *Matter* **2022**, *5*, 4379−4395.
(106) Sakuda, A.; Yamauchi, A.; Yubuchi, S.; Kitamura, N.; Idemoto, Y.; Hayashi, A.; Tatsumisago, M. Mechanochemically Prepared Li_2S-P_2S_5-$LiBH_4$ Solid Electrolytes with an Argyrodite Structure. *ACS Omega* **2018**, *3*, 5453−5458.
(107) Maughan, A. E.; Ha, Y.; Pekarek, R. T.; Schulze, M. C. Lowering the Activation Barriers for Lithium-Ion Conductivity through Orientational Disorder in the Cyanide Argyrodite Li_6PS_5CN. *Chem. Mater.* **2021**, *33*, 5127−5136.
(108) Ray, C. E.; Yao, Y.; Galinat, S. L.; Addison, B.; Blum, V.; Maughan, A. E. Site Disorder Drives Cyanide Dynamics and Fast Ion Transport in Li_6PS_5CN. *Chem. Mater.* **2024**, *36*, 9424−9441.
(109) Koch, B.; Kong, S. T.; Gün, O.; Deiseroth, H.-J.; Eckert, H. Site Preferences and Ion Dynamics in Lithium Chalcohalide Solid Solutions with Argyrodite Structure: II. Multinuclear Solid State NMR of the Systems $Li_6PS_{5-x}Se_xCl$ and $Li_6PS_{5-x}Se_xBr$. *Z. Phys. Chem.* **2022**, *236*, 875−898.
(110) Schlem, R.; Ghidiu, M.; Culver, S. P.; Hansen, A.-L.; Zeier, W. G. Changing the Static and Dynamic Lattice Effects for the Improvement of the Ionic Transport Properties within the Argyrodite $Li_6PS_{5-x}Se_xI$. *ACS Appl. Energy Mater.* **2020**, *3*, 9−18.
(111) Kimura, T.; Izawa, R.; Hotehama, C.; Fujii, K.; Sakuda, A.; Yashima, M.; Tatsumisago, M.; Hayashi, A. Synthesis and Ionic Conductivity of an Argyrodite-Type Li_6SbS_5I Electrolyte. *Solid State Ion.* **2023**, *399*, 116287.
(112) Rice, M. J.; Roth, W. L. Ionic Transport in Super Ionic Conductors: A Theoretical Model. *J. Solid State Chem.* **1972**, *4*, 294−310.
(113) Funke, K. Jump Relaxation in Solid Electrolytes. *Prog. Solid State Chem.* **1993**, *22*, 111−195.
(114) Funke, K. Ion Transport in Fast Ion Conductors — Spectra and Models. *Solid State Ion.* **1997**, *94*, 27−33.
(115) Heitjans, P.; Kärger, J., Eds. *Diffusion in Condensed Matter: Methods, Materials, Models*; Springer: Berlin, Heidelberg, 2005.
(116) Bachman, J. C.; Muy, S.; Grimaud, A.; Chang, H.-H.; Pour, N.; Lux, S. F.; Paschos, O.; Maglia, F.; Lupart, S.; Lamp, P.; et al. Inorganic Solid-State Electrolytes for Lithium Batteries: Mechanisms and Properties Governing Ion Conduction. *Chem. Rev.* **2016**, *116*, 140−162.
(117) Ohno, S.; Banik, A.; Dewald, G. F.; Kraft, M. A.; Krauskopf, T.; Minafra, N.; Till, P.; Weiss, M.; Zeier, W. G. Materials Design of Ionic Conductors for Solid State Batteries. *Prog. Energy* **2020**, *2*, 022001.
(118) Vineyard, G. H. Frequency Factors and Isotope Effects in Solid State Rate Processes. *J. Phys. Chem. Solids* **1957**, *3*, 121−127.
(119) Tilley, R. J. D. *Defects in Solids*; John Wiley & Sons, Inc, 2008.
(120) Muy, S.; Schlem, R.; Shao-Horn, Y.; Zeier, W. G. Phonon−Ion Interactions: Designing Ion Mobility Based on Lattice Dynamics. *Adv. Energy Mater.* **2021**, *11*, 2002787.
(121) Murch, G. E. The Haven Ratio in Fast Ionic Conductors. *Solid State Ion.* **1982**, *7*, 177−198.
(122) Popov, I.; Biernacka, K.; Zhu, H.; Nti, F.; Porcarelli, L.; Wang, X.; Khamzin, A.; Gainaru, C.; Forsyth, M.; Sokolov, A. P. Strongly Correlated Ion Dynamics in Plastic Ionic Crystals and Polymerized Ionic Liquids. *J. Phys. Chem. C* **2020**, *124*, 17889−17896.

https://doi.org/10.1021/acs.chemmater.5c02939
Chem. Mater. 2026, 38, 3038−3058

(123) Vargas-Barbosa, N. M.; Roling, B. Dynamic Ion Correlations in Solid and Liquid Electrolytes: How Do They Affect Charge and Mass Transport? *ChemElectrochem* **2020**, *7*, 367−385.
(124) Payne, B. T.; Juelsholt, M.; Pérez-Osorio, M. A.; Melvin, D. L. R.; Cuello, G. J.; Suard, E.; Irving, D. J. M.; Rees, N. H.; Feaviour, M.; Petrucco, E.; et al. How Multi-Length Scale Disorder Shapes Ion Transport in Lithium Argyrodites. *Energy Environ. Sci.* **2025**, *18*, 8876−8888.
(125) Hanghofer, I.; Brinek, M.; Eisbacher, S. L.; Bitschnau, B.; Volck, M.; Hennige, V.; Hanzu, I.; Rettenwander, D.; Wilkening, H. M. Substitutional Disorder: Structure and Ion Dynamics of the Argyrodites Li_6PS_5Cl, Li_6PS_5Br and Li_6PS_5I. *Phys. Chem. Chem. Phys.* **2019**, *21*, 8489−8507.
(126) Catlow, C. R. A. Static Lattice Simulation of Structure and Transport in Superionic Conductors. *Solid State Ion.* **1983**, *8*, 89−107.
(127) Boyce, J. B.; Huberman, B. A. Superionic Conductors: Transitions, Structures, Dynamics. *Phys. Rep.* **1979**, *51*, 189−265.
(128) Huberman, B. A.; Boyce, J. B. Breakdown of Absolute Rate Theory and Prefactor Anomalies in Superionic Conductors. *Solid State Commun.* **1978**, *25*, 759−762.
(129) Morgan, B. J.; Madden, P. A. Relationships between Atomic Diffusion Mechanisms and Ensemble Transport Coefficients in Crystalline Polymorphs. *Phys. Rev. Lett.* **2014**, *112*, 145901.
(130) Wei, C.; Yu, C.; Wang, R.; Peng, L.; Chen, S.; Miao, X.; Cheng, S.; Xie, J. Sb and O Dual Doping of Chlorine-Rich Lithium Argyrodite to Improve Air Stability and Lithium Compatibility for All-Solid-State Batteries. *J. Power Sources* **2023**, *559*, 232659.
(131) Hogrefe, K.; Hanghofer, I.; Wilkening, H. M. R. with a Little Help from ^{31}P NMR: The Complete Picture on Localized and Long-Range Li^+ Diffusion in Li_6PS_5I. *J. Phys. Chem. C* **2021**, *125*, 22457−22463.
(132) Zhou, L.; Minafra, N.; Zeier, W. G.; Nazar, L. F. Innovative Approaches to Li-Argyrodite Solid Electrolytes for All-Solid-State Lithium Batteries. *Acc. Chem. Res.* **2021**, *54*, 2717−2728.
(133) Hartel, J.; Banik, A.; Gerdes, J. M.; Wankmiller, B.; Helm, B.; Li, C.; Kraft, M. A.; Hansen, M. R.; Zeier, W. G. Understanding Lithium-Ion Transport in Selenophosphate-Based Lithium Argyrodites and Their Limitations in Solid-State Batteries. *Chem. Mater.* **2023**, *35*, 4798−4809.
(134) Gautam, A.; Sadowski, M.; Prinz, N.; Eickhoff, H.; Minafra, N.; Ghidiu, M.; Culver, S. P.; Albe, K.; Fässler, T. F.; Zobel, M.; et al. Rapid Crystallization and Kinetic Freezing of Site-Disorder in the Lithium Superionic Argyrodite Li_6PS_5Br. *Chem. Mater.* **2019**, *31*, 10178−10185.
(135) Lavrinenko, A. K.; Famprikis, T.; Quirk, J. A.; Landgraf, V.; Groszewicz, P. B.; Heringa, J. R.; Smeets, S.; Azizi, V.; Ciarella, S.; Dawson, J. A.; et al. Optimizing Ionic Transport in Argyrodites: A Unified View on the Role of Sulfur/Halide Distribution and Local Environments. *J. Mater. Chem. A* **2024**, *12*, 26596−26611.
(136) Landgraf, V.; Tu, M.; Zhao, W.; Lavrinenko, A. K.; Cheng, Z.; Canals, J.; de Leeuw, J.; Ganapathy, S.; Vasileiadis, A.; Wagemaker, M.; et al. Disorder-Mediated Ionic Conductivity in Irreducible Solid Electrolytes. *J. Am. Chem. Soc.* **2025**, *147*, 18840−18852.
(137) Li, S.; Lin, J.; Schaller, M.; Indris, S.; Zhang, X.; Brezesinski, T.; Nan, C. W.; Wang, S.; Strauss, F. High-Entropy Lithium Argyrodite Solid Electrolytes Enabling Stable All-Solid-State Batteries. *Angew. Chem., Int. Ed.* **2023**, *62*, No. e202314155.
(138) Galinat, S. L.; Willard, C. M.; Valeti, K. T.; Smaha, R. W.; Staerz, A.; Maughan, A. E. Expanding Configurational Complexity through Dipole Dilution in Pseudohalide Argyrodite Ion Conductors. *Chem. Mater.* **2025**, *37*, 9787−9798.
(139) Wei, B.; Sun, Q.; Li, C.; Hong, J. Phonon Anharmonicity: A Pertinent Review of Recent Progress and Perspective. *Sci. China Phys. Mech. Astron.* **2021**, *64*, 117001.
(140) Böer, K. W.; Pohl, U. W. *Semiconductor Physics*; Springer International Publishing: Cham, 2018; pp. 151−179.
(141) Wakamura, K. Roles of Phonon Amplitude and Low-Energy Optical Phonons on Superionic Conduction. *Phys. Rev. B: Condens. Matter.* **1997**, *56*, 11593−11599.
(142) Wang, C.; Xu, B. B.; Zhang, X.; Sun, W.; Chen, J.; Pan, H.; Yan, M.; Jiang, Y. Ion Hopping: Design Principles for Strategies to Improve Ionic Conductivity for Inorganic Solid Electrolytes. *Small* **2022**, *18*, 2107064.
(143) Shen, X.; Koza, M. M.; Tung, Y.-H.; Ouyang, N.; Yang, C.-C.; Wang, C.; Chen, Y.; Willa, K.; Heid, R.; Zhou, X.; Weber, F.; et al. Soft Phonon Mode Triggering Fast Ag Diffusion in Superionic Argyrodite Ag_8GeSe_6. *Small* **2023**, *19*, 2305048.
(144) Silverman, B. D. Collision-Broadened Phonon Line Shape in the Overdamped or Hydrodynamic Regime. *Phys. Rev. B: Condens. Matter.* **1974**, *9*, 203−208.
(145) Ghata, A.; Eckert, P. L.; Böger, T.; Garg, P.; Zeier, W. G. Influence of Cu^+ Substitution on the Structural, Ionic, and Thermal Transport Properties of $Ag_{8-x}Cu_xGeS_6$ Argyrodites. *Chem. Mater.* **2025**, *37* (17), 6900−6911.
(146) Gaudin, E.; Boucher, F.; Petricek, V.; Taulelle, F.; Evain, M. Structures and Phase Transitions of the A_7PSe_6 (A = Ag, Cu) Argyrodite-Type Ionic Conductors. II. β- and β-Cu_7PSe_6. *Acta Crystallogr. B* **2000**, *56*, 402−408.
(147) Gaudin, E.; Petricek, V.; Boucher, F.; Taulelle, F.; Evain, M. Structures and Phase Transitions of the A_7PSe_6 (A = Ag, Cu) Argyrodite-Type Ionic Conductors. III. α-Cu_7PSe_6. *Acta Crystallogr. B* **2000**, *56*, 972−979.
(148) Böger, T.; Strotmann, K.; Faka, V.; Maus, O.; Abernathy, D. L.; Granroth, G. E.; Jalarvo, N. H.; Li, C.; Suard, E.; Zeier, W. G. Impact of Structural Coherence and Disorder on the Ionic Transport and Lattice Dynamics in Li^+-Conducting Argyrodites. *J. Mat. Chem. A* **2025**, *13* (45), 39211−39228.
(149) Ding, J.; Gupta, M. K.; Rosenbach, C.; Lin, H.-M.; Osti, N. C.; Abernathy, D. L.; Zeier, W. G.; Delaire, O. Liquid-Like Dynamics in a Solid-State Lithium Electrolyte. *Nat. Phys.* **2025**, *21*, 118−125.
(150) Wakamura, K. Origin of the Low-Energy Mode in Superionic Conductors. *Phys. Rev. B: Condens. Matter.* **1999**, *59*, 3560−3568.
(151) Wakamura, K. Effects of Electronic Band on Activation Energy and of Effective Charge on Lattice Distortion in Superionic Conductors. *J. Phys. Chem. Solids* **1998**, *59*, 591−598.
(152) Wakamura, K. Correlation Between High Ionic Conduction and Anomaly of Dielectric Property. *Solid State Commun.* **1993**, *86*, 503−507.
(153) Jonscher, A. K. Dielectric Relaxation with Dipolar Screening. *J. Mater. Sci.* **1997**, *32*, 6409−6414.
(154) Bernges, T.; Culver, S. P.; Minafra, N.; Koerver, R.; Zeier, W. G. Competing Structural Influences in the Li Superionic Conducting Argyrodites $Li_6PS_{5-x}Se_xBr$ $(0 \leq x \leq 1)$ upon Se Substitution. *Inorg. Chem.* **2018**, *57*, 13920−13928.
(155) Kittel, C. *Introduction to Solid State Physics*; Wiley: Hoboken, NJ, 2005.
(156) Garai, J. Physics Behind the Debye Temperature. *arXiv*. 2009; http://arxiv.org/abs/physics/0703001.
(157) Li, X.; Liu, H.; Zhao, C.; Kim, J. T.; Fu, J.; Hao, X.; Li, W.; Li, R.; Chen, N.; Cao, D.; et al. Hopping Rate and Migration Entropy as the Origin of Superionic Conduction within Solid-State Electrolytes. *J. Am. Chem. Soc.* **2023**, *145*, 11701−11709.
(158) Almond, D. P.; Hunter, C. C.; West, A. R. The Extraction of Ionic Conductivities and Hopping Rates from A.C. Conductivity Data. *J. Mater. Sci.* **1984**, *19*, 3236−3248.
(159) Muy, S.; Bachman, J. C.; Chang, H.-H.; Giordano, L.; Maglia, F.; Lupart, S.; Lamp, P.; Zeier, W. G.; Shao-Horn, Y. Lithium Conductivity and Meyer-Neldel Rule in Li_3PO_4-Li_3VO_4-Li_4GeO_4 Lithium Superionic Conductors. *Chem. Mater.* **2018**, *30*, 5573−5582.
(160) Ngai, K. L. Meyer-Neldel Rule and Anti Meyer-Neldel Rule of Ionic Conductivity: Conclusions from the Coupling Model. *Solid State Ion.* **1998**, *105*, 231−235.
(161) Kraft, M. A.; Ohno, S.; Zinkevich, T.; Koerver, R.; Culver, S. P.; Fuchs, T.; Senyshyn, A.; Indris, S.; Morgan, B. J.; Zeier, W. G. Inducing High Ionic Conductivity in the Lithium Superionic Argyrodites $Li_{6+x}P_{1-x}Ge_xS_5I$ for All-Solid-State Batteries. *J. Am. Chem. Soc.* **2018**, *140*, 16330−16339.

(162) Shannon, R. D.; Prewitt, C. T. Effective Ionic Radii in Oxides and Fluorides. *Acta Crystallogr.* **1969**, *25*, 925−946.
(163) Culver, S. P.; Koerver, R.; Krauskopf, T.; Zeier, W. G. Designing Ionic Conductors: The Interplay between Structural Phenomena and Interfaces in Thiophosphate-Based Solid-State Batteries. *Chem. Mater.* **2018**, *30*, 4179−4192.
(164) Wang, Y.; Richards, W. D.; Ong, S. P.; Miara, L. J.; Kim, J. C.; Mo, Y.; Ceder, G. Design Principles for Solid-State Lithium Superionic Conductors. *Nat. Mater.* **2015**, *14*, 1026−1031.
(165) Wood, B. C.; Varley, J. B.; Kweon, K. E.; Shea, P.; Hall, A. T.; Grieder, A.; Ward, M.; Aguirre, V. P.; Rigling, D.; Lopez Ventura, E.; et al. Paradigms of Frustration in Superionic Solid Electrolytes. *Phil. Trans. R. Soc. A* **2021**, *379*, 20190467.
(166) Secco, E. A. Ion Transport in Sulfates: Percolation Mechanism Versus Paddle-Wheel Mechanism. *Solid State Commun.* **1988**, *66*, 921−923.
(167) Secco, E. A. Paddle-Wheel Versus Percolation Model. *Solid State Ion.* **1993**, *60*, 233−235.
(168) Karlsson, L.; McGreevy, R. L. Mechanisms of Ionic Conduction in Li_2SO_4 and $LiNaSO_4$: Paddle Wheel or Percolation? *Solid State Ion.* **1995**, *76*, 301−308.
(169) O'Leary, G. P.; Wheeler, R. G. Phase Transitions and Soft Librational Modes in Cubic Crystals. *Phys. Rev. B* **1970**, *1*, 4409−4439.
(170) Armstrong, R. L. Displacive Order-Disorder Crossover in Perovskite and Antifluorite Crystals Undergoing Rotational Phase Transitions. *Prog. Nucl. Magn. Reson. Spectrosc.* **1989**, *21*, 151−173.
(171) Smith, J. G.; Siegel, D. J. Ion Migration Mechanisms in the Sodium Sulfide Solid Electrolyte $Na_{3-x}Sb_{1-x}W_xS_4$. *Chem. Mater.* **2022**, *34*, 4166−4171.
(172) Fang, H.; Jena, P. Argyrodite-Type Advanced Lithium Conductors and Transport Mechanisms Beyond Paddle-Wheel Effect. *Nat. Commun.* **2022**, *13*, 2078.
(173) Hoang, K.; Van de Walle, C. G. Mechanism for the Decomposition of Lithium Borohydride. *Int. J. Hydrogen Energy* **2012**, *37*, 5825−5832.
(174) Lundén, A. Paddle-Wheel Versus Percolation Model, Revisited. *Solid State Ion.* **1994**, *68*, 77−80.
(175) Lundén, A. Evidence for and Against the Paddle-Wheel Mechanism of Ion Transport in Superionic Sulphate Phases. *Solid State Commun.* **1988**, *65*, 1237−1240.
(176) Lundén, A. Enhancement of Cation Mobility in Some Sulphate Phases Due to a Paddle-Wheel Mechanism. *Solid State Ion.* **1988**, *28*−*30*, 163−167.
(177) Andersen, N.; Bandaranayake, P.; Careem, M.; Dissanayake, M.; Wijayasekera, C.; Kaber, R.; Lunden, A.; Mellander, B.; Nilsson, L.; Thomas, J. Paddle-Wheel Versus Percolation Mechanism for Cation Transport in Some Sulphate Phases. *Solid State Ion.* **1992**, *57*, 203−209.
(178) Jun, K.; Lee, B. L.; Kam, R.; Ceder, G. The Nonexistence of a Paddlewheel Effect in Superionic Conductors. *Proc. Natl. Acad. Sci. U. S. A.* **2024**, *121*, No. e2316493121.
(179) Smith, J. G.; Siegel, D. J. Low-Temperature Paddlewheel Effect in Glassy Solid Electrolytes. *Nat. Commun.* **2020**, *11*, 1483.
(180) Smith, J. G.; Siegel, D. J. A Proper Definition of the Paddlewheel Effect Affirms its Existence. *Proc. Natl. Acad. Sci. U. S. A.* **2025**, *122*, No. e2419892122.
(181) Jun, K.; Ceder, G. Reply to Smith and Siegel: Most Lithium Hops in Paddlewheel-Claimed Conductors Occur Without Spatially and Temporally Correlated Anion-Group Rotations. *Proc. Natl. Acad. Sci. U. S. A.* **2025**, *122*, No. e2423194122.
(182) Secco, E. Paddle Wheel Mechanism in Lithium sulfates: Arguments in Defense and Evidence Against. *J. Solid State Chem.* **1992**, *96*, 366−375.
(183) Zhang, Z.; Nazar, L. F. Exploiting the Paddle-Wheel Mechanism for the Design of Fast Ion Conductors. *Nat. Rev. Mater.* **2022**, *7*, 389−405.
(184) Kim, J. H.; Jun, B.; Jang, Y. J.; Choi, S. H.; Choi, S. H.; Cho, S. M.; Kim, Y.-G.; Kim, B.-H.; Lee, S. U. Highly Reliable and Large-Scale Simulations of Promising Argyrodite Solid-State Electrolytes Using a Machine-Learned Moment Tensor Potential. *Nano Energy* **2024**, *124*, 109436.

https://doi.org/10.1021/acs.chemmater.5c02939
Chem. Mater. 2026, 38, 3038−3058